PMEL Tsunami Forecast Series: Vol.
A Tsunami Forecast Model for Christiansted, U.S. Virgin Islands

Hongqiang Zhou [1,2] and NCTR Staff

1. NOAA Center for Tsunami Research, Pacific Marine Environmental Laboratory, Seattle, WA
2. Joint Institute for the Study of the Atmosphere and Ocean, Seattle, WA

Contents

List of Figures

List of Tables

Abstract Based on the Method Of Splitting Tsunami (MOST) numerical model, a tsunami forecast model is developed for the city of Christiansted, U.S. Virgin Islands, centered on Christiansted Harbor. Along with the forecast model, a reference model is also developed at higher resolution and larger spatial coverage. Simulations of several synthetic tsunami events, including extreme scenarios, with the forecast and reference models are performed and analyzed for model validation and associated hazard evaluation. Both models show robust performance. The forecast model for Christiansted is expected to provide an accurate estimate of wave arrival time, wave heights, and inundation extent in approximately 24 minutes of computation.

1 Background and Objectives

The National Oceanic and Atmospheric Administration (NOAA) Center for Tsunami Research (NCTR) at the NOAA Pacific Marine Environmental Laboratory (PMEL) has developed a tsunami forecasting capability for operational use by NOAA's two Tsunami Warning Centers located in Hawaii and Alaska (Titov et al., 2005). The system is designed to provide basin-wide warning of approaching tsunami waves accurately and quickly. The system, termed Short-term Inundation Forecast for Tsunamis (SIFT), combines real-time tsunami event data with numerical models to produce estimates of tsunami wave arrival times and amplitudes at a coastal community of interest. The SIFT system integrates several key components: deep-ocean observations of tsunamis in real time, a basin-wide pre-computed propagation database of water level and flow velocities based on potential seismic unit sources, an inversion algorithm to refine the tsunami source based on deep-ocean observations during an event, and high-resolution tsunami forecast models.

The Virgin Islands are a group of islands in the Caribbean Sea, about 40 miles (64 km) east of Puerto Rico. The archipelago is made up of United States and British territories. The U.S. Virgin Islands consists of the main islands of St. Thomas, St. John, St. Croix and many smaller islands. The total land area of the territory is 133.73 square miles (346.4 sq. km). Christiansted is a town on the north shore of St. Croix, next to Christiansted Harbor (Figure 1). It is a former capital of the Danish West Indies and home to the Christiansted National Historic Site. As of 2010, Christiansted has a population of 2433 (U.S. Census Bureau, 2013).

The U.S. Virgin Islands is at risk of tsunamis that originate from far-field earthquakes across the Atlantic, local earthquakes on the Caribbean subduction zone, and local landslides. This region is believed to have been hit by two tsunamis coming from the Portugal shore in 1755 and 1761, respectively (Grothe et al., 2012). Examples of this region's high seismicity include a magnitude 7.5 earthquake northwest of Puerto Rico in 1943, as well as magnitude 8.1 and 6.9 earthquakes north of Hispaniola in 1946 and 1953, respectively. Some of these earthquakes have generated tsunamis. Eyewitness reports of an 1867 Virgin Islands tsunami gave a maximum wave height of more than 7 m in Frederiksted, a town on the west end of St. Croix, where a large naval vessel was left on top of a pier (`http://woodshole.er.usgs.gov/project-pages/caribbean/`). A magnitude 7.5 earthquake in 1918 resulted in a tsunami that killed at least 40 people in northwestern Puerto Rico. Immediately after the 1946 earthquake, a tsunami had struck northeastern Hispaniola and moved inland for several kilometers. Some reports indicated that nearly 1,800 people had been drowned in this event.

Based on the Method Of Splitting Tsunami (MOST) numerical model, a tsunami forecast model has been developed for the city of Christiansted, centered on Christiansted Harbor. The purpose of this model is to provide this region with accurate and timely information that is necessary to minimize false alarms and make appropriate decisions in the event of tsunami. Development of this model is described in the present report.

2 Forecast Methodology

The SIFT system employs the MOST numerical model (Titov and Synolakis, 1998), which is a set of code for simulating three processes of tsunami evolution: generation by an earth-

quake, transoceanic propagation, and inundation of dry land at specific sites. The forecast is supported by a propagation database, which includes the time series of simulated water surface elevations and water velocities in the oceanic basin due to unit earthquake sources covering worldwide subduction zones (Gica et al., 2008). As the waves propagate across the ocean and reach tsunameter observation sites, the forecast system uses a data inversion technique to deduce the tsunami source in terms of unit earthquake sources (Percival et al., 2009). A linear combination of the pre-computed unit tsunami source functions is then employed to produce synthetic boundary conditions of water elevations and flow velocities for the site-specific forecast models. The main objective of a forecast model is to provide an accurate estimate of wave arrival time, wave height, and inundation extent at a particular location in minutes of computational time. Efficiency and accuracy of forecast models currently implemented in the Pacific region have been validated in recent historical events (Titov et al., 2005; Titov, 2009; Tang et al., 2008; Wei et al., 2008).

3 Model Development

Each forecast model consists of three nested grids with increasing spatial resolutions, referred to as A, B, and C grids. The outer and coarser A grid receives its boundary input of water elevations and flow velocities from the pre-computed database, and provides boundary input of a refined (with respect to the database) solution into the B grid, which is smaller in extent and finer in resolution. The B-grid solution, refined further, provides boundary input into the finest and smallest of the three, the C grid. Within C grid, the solution is expected to be accurate enough to match the major features of a tide gauge tsunami record.

All tsunami forecast models are run in real time while a tsunami is propagating across the open ocean. Thus, computational time is the critical factor for model development. Meeting the time constraint is achieved by manipulating the spatial and temporal resolutions of grids, balancing computational speed with numerical accuracy.

The development of a forecast model is centered around "optimizing" (reducing) the coverage and resolutions of computational grids, so as to effectively reduce computational time without noticeably degrading the numerical solution, more specifically, a time history at an observation point (usually, at a tide gauge location). Time histories computed with optimized grids are evaluated by visual comparison with those obtained from a reference model, which is comprised of grids covering larger areas at higher resolution (Tang et al., 2009).

3.1 Forecast Area

As provided by the U.S. Geological Survey (`http://woodshole.er.usgs.gov/project-pages/caribbean/`), Puerto Rico, the Virgin Islands, and Hispaniola Island are located on an active plate boundary zone between the North American plate and the northeast corner of the Caribbean plate (Figure 2). The Caribbean plate slides eastward at approximately 2 cm/yr relative to the North American plate with a small component of subduction (one plate sinks under the other plate). In contrast, the Caribbean plate farther east overrides the North American plate, creating the island arc of the Lesser Antilles. There are no active volcanoes in the Virgin Islands, though most of the islands are volcanic in origin.

Because Puerto Rico and the Virgin Islands are located at an active plate boundary, earthquakes are a constant threat, and the densely populated coastal areas are vulnerable to tsunamis. The U.S. Geological Survey indicates that all of the known causes of tsunamis are present in the Caribbean region – earthquakes, submarine landslides, submarine volcanic eruptions, as well as transoceanic tsunamis from distant sources (`http://pubs.usgs.gov/of/1999/of99-353/`). The city of Christiansted, the subject of this report, is located on the north shore of the island of St. Croix.

A tide gauge maintained by the National Ocean Service (NOS) is located on the docks in Gallows Bay on the east side of Christiansted Harbor (17°45′N, 64°42.3′W). An image of this tide gauge is shown in Figure 3, and its location is presented in Figure 4. A sample record obtained by this gauge in March 2012 is shown in Figure 5. After the tidal components were removed through a high-pass Butterworth filter using a 3-hr cut-off period, the average power spectrum of the residual (background signal) was computed to detect normal oscillations of the harbor, if any. The average power spectrum, shown in Figure 6, was computed through the Discrete Fourier Transform of a selected fragment from the month-long record (Tolkova and Power, 2011). The fragment has a length of 12.8 hr, which limits the frequency resolution to 0.08 cycles/hr, though the Discrete Fourier Transform is computed with a 0.04-cycles/hr increment. Due to a 6-min sampling rate, frequencies above the tidal range but under 5 cycles/hr, or periods from 12 min to 3 hr, are of interest. The gauge background spectrum appears to be dominated by wide-band long-wave noises due to fluctuations of atmospheric pressure. This analysis has not detected distinct oscillations essential for tsunami wave dynamics. There is no instrumental record of historical tsunamis in this area.

3.2 Model Setup

3.2.1 Bathymetry Sources

The bathymetry and topography data used in the development of this forecast model are based on digital elevation models (DEMs) provided by the National Geophysical Data Center (NGDC). The authors assume that these data adequately represent the local topography/bathymetry. As new DEMs become available, forecast models will be updated and reported at `http://nctr.pmel.noaa.gov/forecast_reports/`.

The bathymetric data in the forecast model A grid are derived from the 9-arc-sec Gulf Coast/Caribbean DEM and the Virgin Islands DEM of 1-arc-sec resolution. The Gulf Coast/Caribbean grid is compiled from a variety of sources (NGDC, 2005). Occasional visible mismatch between different sources has been observed in some areas, where smoothing was performed. The different sources have not been converted to a common vertical datum. Mean Sea Level is the assumed vertical reference. No topographic data are contained in this grid. The two datasets poorly match with each other in shallow areas around the Virgin Islands. The Virgin Islands DEM is more realistic and therefore is employed in the shallow areas. The 9-arc-sec Gulf Coast/Caribbean data are used in deeper water areas where the 1-arc-sec Virgin Islands DEM data are not available. The B grid is cut from the Virgin Islands DEM. The C grid is cut from the St. Croix DEM of 1/3-arc-sec resolution. A low-pass Butterworth filter has been applied to this source grid in order to avoid aliasing when it is re-sampled to the desired resolution. Both B and C grids are referenced to Mean

High Water to model "worst-case scenario" flooding (Grothe et al., 2012).

3.2.2 Grid Selection

The forecast model solution for the Virgin Islands area is sensitive to the outer (A) grid coverage. Because the islands and underwater ridges act as reflectors and waveguides, wave energy is redistributed toward later waves. To accurately simulate the amplitudes along a wave train, the outer grid should include the essential bathymetric features. The outer grid extends far enough west of Puerto Rico to include the east tip of Hispaniola Island, and far enough south to include the underwater flats (Figure 7). The reference A grid has a coverage of 2.9° (16.05–18.95°N) × 9.4° (69.9–60.5°W), which is equivalent to an area of 322.8 km × 996.8 km. The optimized A grid has a coverage of 2.45° (16.5–18.95°N) × 8.0° (69–61°W), or 272.7 km × 848.3 km. The reference A grid has a resolution of 20 arc sec, which is finer than the 45 arc sec in the optimized A grid.

Specific to St. Croix, tsunamis may propagate onto the island as shelf waves. Near Christiansted, tsunamis are likely to excite standing waves on the north side of the shelf to the east of the forecast area. This wave formation is likely to happen in the B grid. Therefore, the essential bathymetric features responsible for local resonance need to be included and resolved in this grid. The reference B grid has a coverage of 0.25° (17.6-17.85°N) × 0.55° (64.95–64.4°W), or an area of 27.83 km × 58.36 km, surrounding the entire island and the shelf. The coverage of the optimized B grid is 0.12° (17.73–17.85°N) × 0.34° (64.76–64.42°W), which is equivalent to an area of 13.36 km × 36.05 km. Both grids have the same resolution of 4 arc sec so as to accurately represent shelf features.

The purpose of C grid is to refine the corresponding B-grid solution and to provide an inundation forecast for a locality. Thus, a B-grid solution provides the starting point from which refinements are to be made. In our case, since the B-grid resolution is relatively high, a C-grid solution in water is expected to be close to that computed in the B grid for a wide range of C-grid parameters such as coverage and resolution. Reference C grid was selected with a coverage of 0.0167° (17.7420–17.7587°N) × 0.0546° (64.7300–64.6754°W), or 1.855 km × 5.792 km at a resolution of 1/3 arc sec in both longitude and latitude. The optimized C grid has a reduced coverage, i.e., 0.017° (17.742–17.759°N) × 0.034° (64.73–64.696°W), or 1.892 km × 3.605 km. The resolution of this grid is 2/3 arc sec.

Grid coverage, resolutions, and length of time steps of both reference and forecast models are given in Table 1. Boundaries and bathymetry of all grids are also shown in Figures 7–9. Computational parameters of the two models are given in Appendix A. In the forecast model, as well as in the reference model, time series of computed wave elevations are read on a reference grid node that is nearest to the actual location of the tide gauge. Water depth is 3.8 m at this grid node in both models.

4 Results and Discussion

To assess the accuracy and stability of the forecast model, as well as to infer tsunami behavior and the extent of associated hazards, we employ a number of synthetic scenarios, which include six mega tsunamis, a unit tsunami, and a micro tsunami. The event sources are selected to represent different locations within the Atlantic (Caribbean) subduction zone

(ATSZ) and the South Sandwich subduction zone (SSSZ). A mega-tsunami event originates from 20 unit sources, in which distributes a uniform slip of 25 m, equivalent to a moment magnitude (Mw) 9.3 earthquake. The unit-tsunami event involves one unit source in ATSZ with a slip of 1.0 m, equivalent to a Mw 7.5 earthquake. The micro tsunami originates from a unit source in SSSZ with a slip of 0.01 m. Parameters of the synthetic scenarios are listed in Table 2. Origins of synthetic mega-tsunami events are shown in Figure 10. A comprehensive description of unit sources in the ATSZ and SSSZ can be found in Appendix B.

4.1 Validation

Figures 11–16 show the maximum water surface elevations with respect to still sea level in grids B and C, as well as time series at the reference grid nodes for the mega-tsunami events. Very good agreement is observed between the reference and the forecast models. In the unit-tsunami event (Figure 17), comparison indicates considerable difference between the two models in computed maximum water surface elevations. This difference is mainly due to the trailing waves of high wave amplitudes and frequencies, as shown in the time series at the reference grid nodes. Computational accuracy for the high-frequency trailing waves is more sensitive to grid resolution because of their relatively short wavelengths. In a tsunami event, maximum inundation along the shoreline is usually caused by the leading low-frequency waves. Therefore, computational errors in the trailing waves due to lower resolution in the optimized grids are unlikely to cause severe mistakes in inundation forecast.

In the absence of records of any actual tsunamis at this location, validity of the forecast model is deduced from the following:

- The MOST numerical model has been proven to simulate tsunami propagation and runup correctly for numerous locations and events throughout the world, and given that nearshore tsunami wave propagation and transformation is governed by the same physical laws at any location;
- the proper choice of numerical parameters for the Christiansted model (such as the model coverage, as well as spatial and temporal resolutions) is fully considered as described in this report;
- the general wave patterns and time histories near the coast, as evaluated with the reference and the forecast models, are consistent with each other.

Therefore it is expected that the forecast model for Christiansted is capable of providing an accurate estimate of wave arrival time, wave height, and inundation extent. The forecast model is configured to run 10-hr simulations in order to capture the trailing waves of considerable amplitudes that may arrive later. A 10-hr simulation requires approximately 24 min of computational time as tested on a 2×2.93 GHz Intel Xeon 6-core workstation working in Red Hat Enterprise Linux Client release 5.11 environment.

Because of the steep shores encircling Christiansted Harbor, a tsunami is not expected to cause significant inundation. Maximum inundation in the most devastating event, ATSZ 48-57 which originate in an immediate vicinity of the forecast area, is shown in Figure 18. The major inundated area is the low-laying sandy beach on the west side of a small island in the center of the harbor.

4.2 Stability

The forecast model is tested for six mega-tsunami scenarios, which represent the extremely severe events that may affect this area. In reality, such an event has not happened in the Atlantic basin in past centuries. Numerical stability is maintained through all these tests. Robustness of the forecast model is further proved in the unit-tsunami event, which may be more frequently experienced in this area. For the real-time simulation to be triggered, incoming wave amplitudes need to exceed a certain threshold along the boundaries of the A grid, which is set to 0.01 m in the present forecast model. This configuration is to prevent the very weak, nonthreatening events from consuming valuable computational resources. To investigate the performance of the forecast model in extreme situations, we temporarily lower this threshold to 0.001 mm and simulate the micro-tsunami event. Numerical stability is also maintained for this scenario. All these tests suggest that the present model is quite robust, and is unlikely to fail in operational tsunami forecasts if integrated into the SIFT system.

5 Conclusions

This report documents the development of a tsunami forecast model for Christiansted, U.S. Virgin Islands. The model is to be integrated into NOAA's SIFT system that provides real-time forecast of tsunami arrival time, wave heights and coastal inundation for at-risk U.S. coastal communities. The core of the forecast model is a numerical model, which consists of three nested grids that transition real-time simulations from deep-water tsunami propagation into nearshore wave evolution and runup at gradually increasing grid resolutions. The grids are constructed with the best available bathymetric and topographic datasets. Grid coverage and resolutions are configured based on the balance between computational efficiency and numerical accuracy. The economic and population center of Christiansted is covered by the innermost grid at a resolution of ~ 20 m. The model is designed to complete a 10-hr simulation within ~ 24 min on a 2×2.93 GHz Intel Xeon 6-core workstation.

Due to the lack of historical tsunami data in this region, the validity of the present forecast model is investigated through synthetic scenarios. These scenarios are computed with both the forecast model and a reference model consisting of grids covering larger domains at higher resolutions. Comparison of computational results between the two models indicates that the forecast model has due accuracy for its design purpose. No stability issue is noticed in the numerical experiments. Therefore, we expect that the forecast model will be a reliable tool with regards to both accuracy and stability if integrated into the SIFT system and deployed for operations.

6 Acknowledgments

The early works on model development and report drafting were taken by E. Tolkova at NCTR. This publication is funded by the Joint Institute for the Study of the Atmosphere and Ocean (JISAO) under NOAA Cooperative Agreement No. NA17RJ1232, Contribution No. 2453. This work is also of Pacific Marine Environmental Laboratory (PMEL) Contribution No. 3379.

References

Gica E., Spillane, M.C., Titov, V.V., Chamberlin, C.D. and Newman, J.C. (2008): Development of the forecast propagation database for NOAA's Short-Term Inundation Forecast for Tsunamis (SIFT), NOAA Tech. Memo. OAR PMEL-139, 89pp.

Grothe, P.R., Taylor, L.A., Eakins, B.W., Carignan, K.S., Caldwell, R.J., Lim, E., and Friday, D.Z. (2012): Digital Elevation Models of the U.S. Virgin Islands: Procedures, Data Sources and Analysis, NOAA Technical Memorandum NESDIS NGDC-55, U.S. Dept. of Commerce, Boulder, CO, 50 pp.

National Geophysical Data Center (NGDC) (2005): East coast and Gulf Coast and Caribbean nine second tsunami propagation grids compilation report, 11 pp., http://onda.pmel.noaa.gov/atlas/citation/10/9sec_intermediate_sub.doc

Percival, D.B., Denbo, D.W., Eble, M.C., Gica, E., Mofjeld, H.O., Spillane, M.C., Tang, L., and Titov, V.V. (2009): Extractiion of tsunami source coefficients via inversion of DART buoy data, Nat. Hazards, 58(1), doi:10.1007/s11069-010-9688-1, 567–590.

Tang, L., Titov, V.V. , Wei, Y., Mofjeld, H.O., Spillane, M., Arcas, D., Bernard, E.N., Chamberlin, C.D., Gica, E., and Newman, J. (2008): Tsunami forecast analysis for the May 2006 Tonga tsunami. J. Geophys. Res., 113, C12015, doi: 10.1029/2008JC004922.

Tang L., Titov, V.V., and Chamberlin, C.D. (2009): Development, testing, and applications of site-specific tsunami inundation models for real-time forecasting. J. Geophys. Res., 114, C12025, doi: 10.1029/2009JC005476.

Titov V.V., and Synolakis, C.E. (1998): Numerical Modeling of Tidal Wave Runup, J. Waterway, Port, Coastal and Ocean Eng., 124(N4), 157–171.

Titov V.V., González, F.I., Bernard, E.N., Eble, M.C., Mofjeld, H.O., Newman, J.C., and Venturato, A.J. (2005): Real-Time Tsunami Forecasting: Challenges and Solutions, Natural Hazards, 35, 41–58.

Titov, V.V. (2009): Tsunami forecasting, in: The Sea, Volume 15: Tsunamis, Harvard University Press, Cambridge, MA and London, England, 371-400.

Tolkova, E., and Power, W. (2011): Obtaining natural oscillatory modes of bays and harbors via Empirical Orthogonal Function analysis of tsunami wave fields. Ocean Dynamics, 61/6, 731–751, doi: 10.1007/s10236-011-0388-5

Tolkova, E. (2013): Tsunami Forecast Model for Charlotte Amalie, VI. NOAA Tech Memo. `http://nctr.pmel.noaa.gov/forecast_reports/draft_reports/CharlotteAmeliaSIM_rev2appC.pdf`

Wei, Y., Bernard, E.N., Tang, L., Weiss, R., Titov, V.V., Moore, C., Spillane, M., Hopkins, M., and Kânŏglu, U. (2008): Real-time experimental forecast of the Peruvian tsunami of August 2007 for U.S. coastlines. Geophys. Res. Lett., 35, L04609, doi: 10.1029/2007GL032250.

U.S. Census Bureau (2013): 2010 Census for U.S. Virgin Islands, CPH-T-8, Population, Housing Units, Land Area, and Density for U.S. Island Areas: 2010, Washington, DC.

Figure 1: Christiansted, U.S. Virgin Islands. Facing north. Photo by Jason P. Heym, taken on the slopes of Recovery Hill.

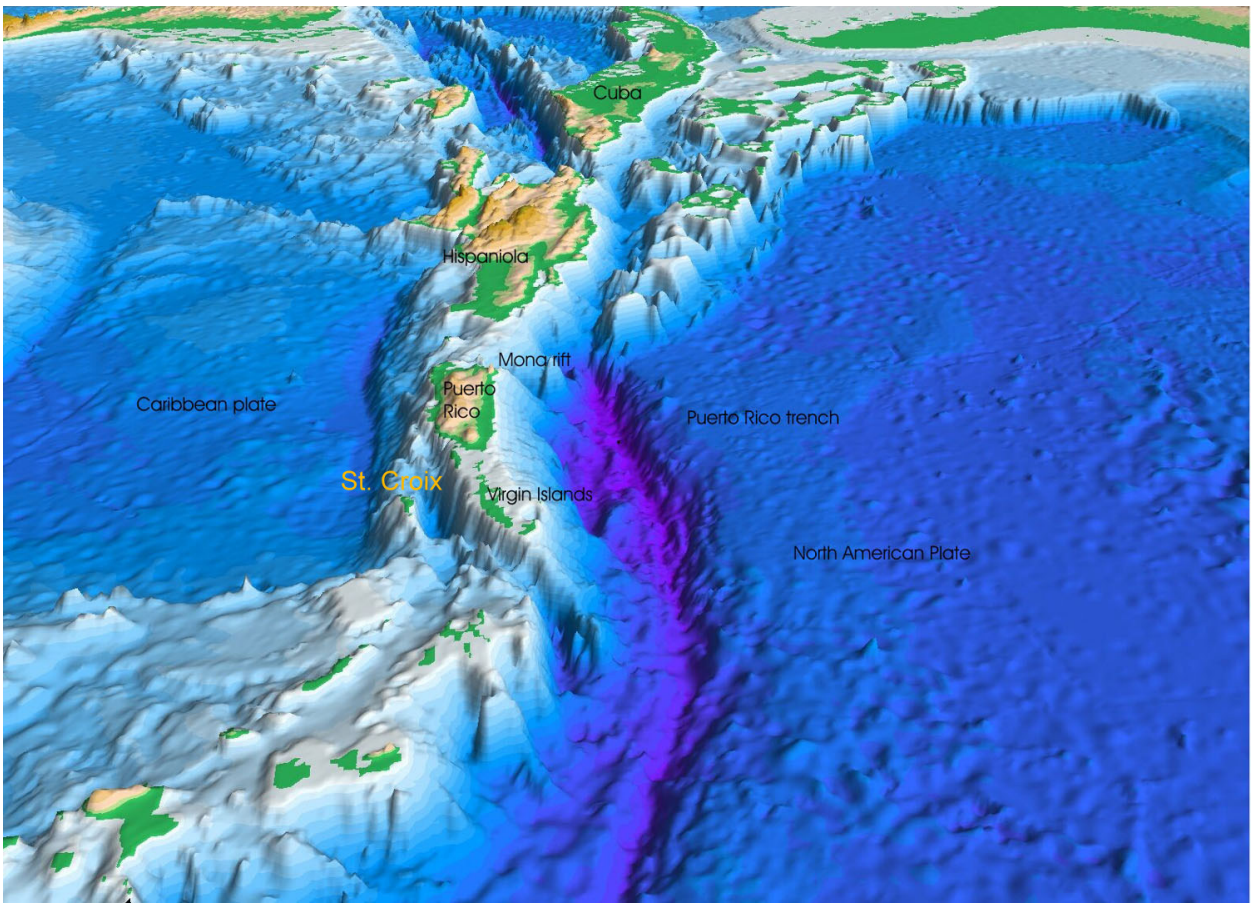

Figure 2: Perspective view of the sea floor of the Atlantic Ocean and the Caribbean Sea. The Lesser Antilles are on the lower left side of the view; Florida is on the upper right; the Puerto Rico trench (purple) is at the center. South to north is left to right. Christiansted is located on the north shore of the island of St. Croix. Courtesy of the U.S. Geological Survey.

Figure 3: The Christiansted Harbor tide gauge (courtesy of NOAA/NOS, `http://tidesandcurrents.noaa.gov`).

Figure 4: Location of the Christiansted Harbor tide gauge (courtesy of Google Maps).

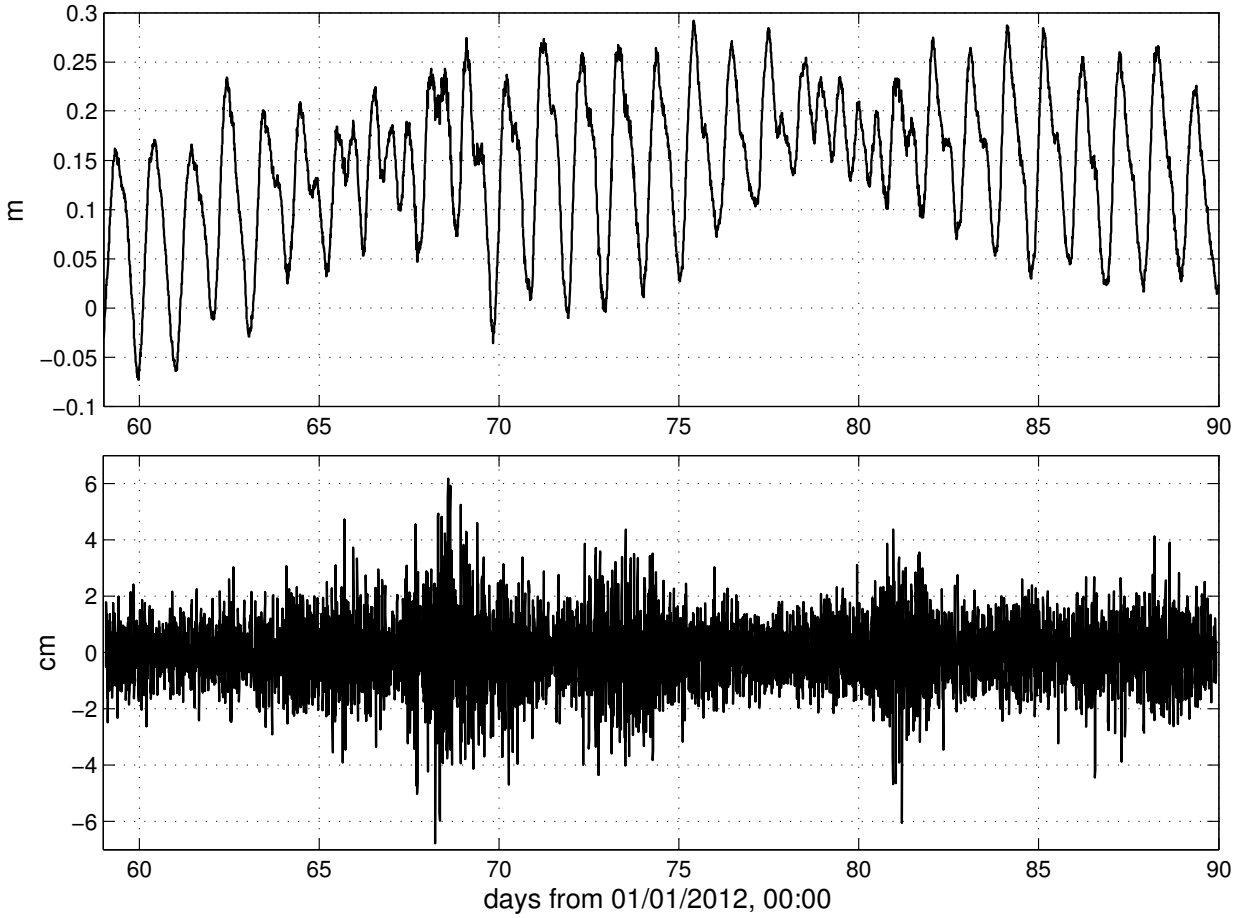

Figure 5: Top: a record of the Christiansted Harbor tide gauge for the month of March 2012 (`http://tidesandcurrents.noaa.gov`). Bottom: residual in the above record, after tidal components were removed using a Butterworth filter with 3 hr cut-off period.

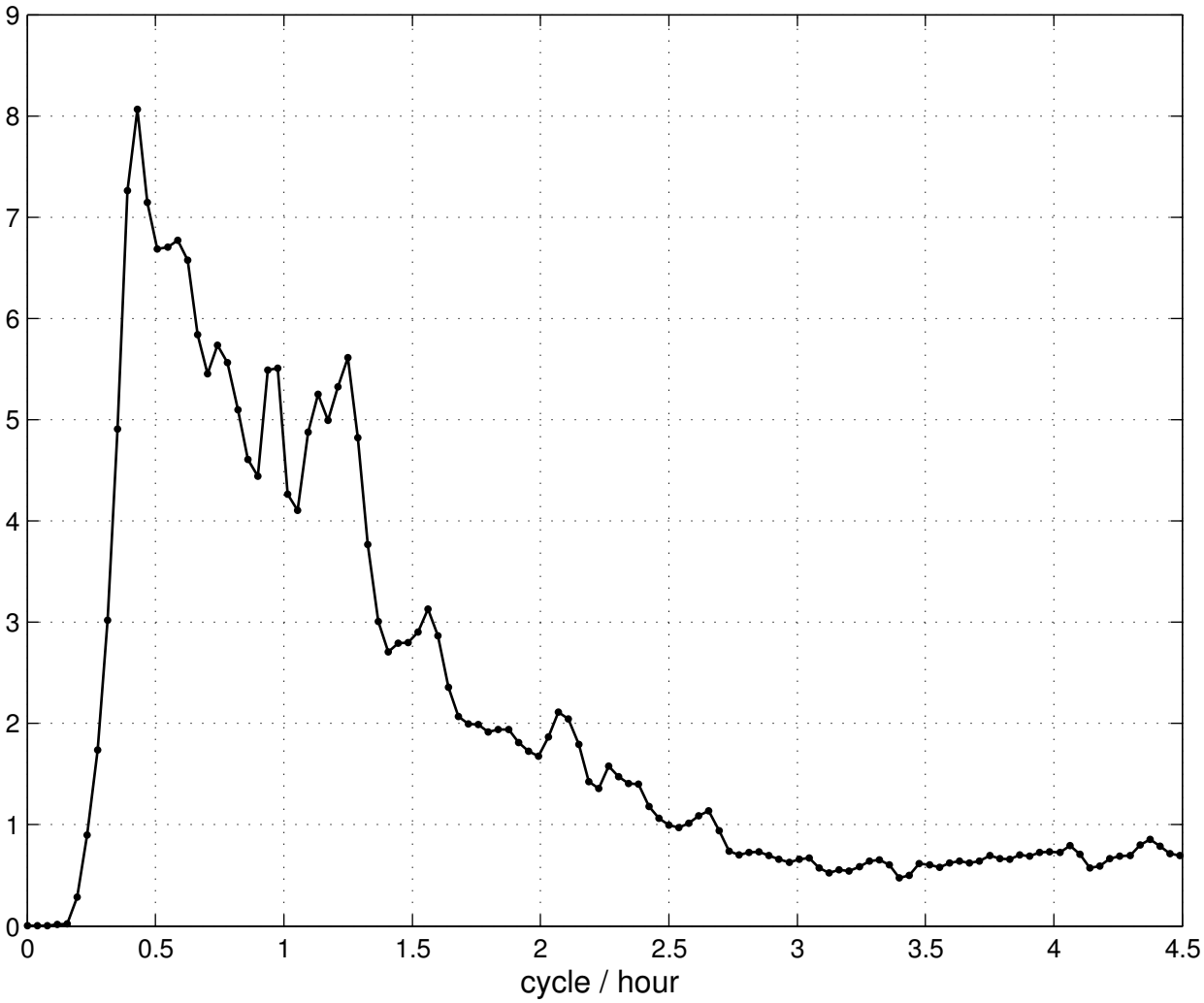

Figure 6: Power spectrum of the gauge background signal for the month of March 2012.

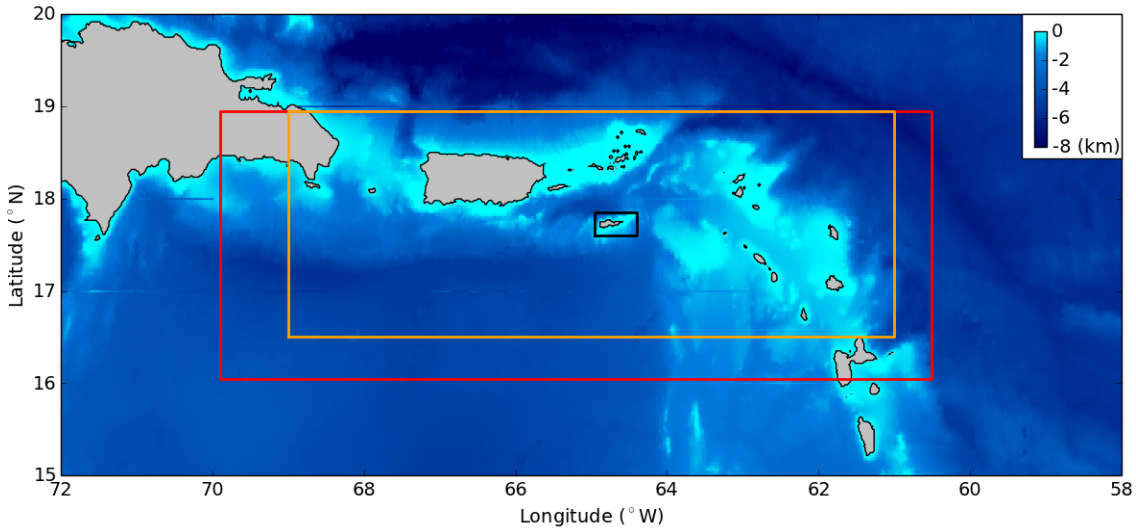

Figure 7: Contours of reference A (red), optimized A (orange), and reference B (black) grids.

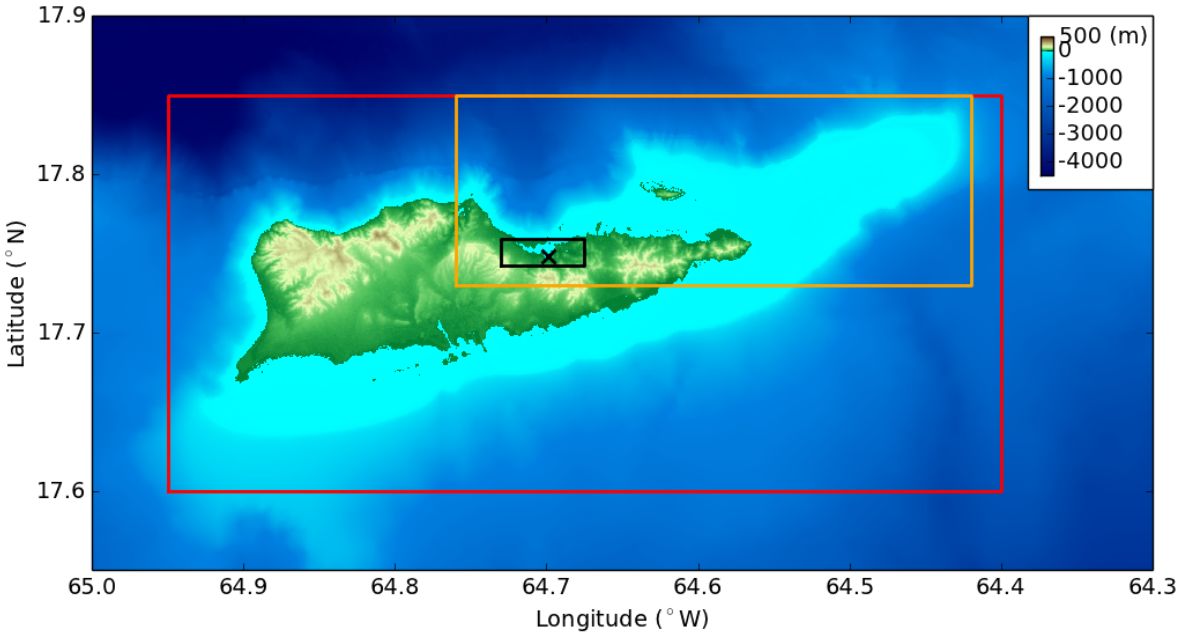

Figure 8: Contours of reference B (red) and optimized B (orange) grids, as well as reference C grid (black). The black × indicates the tide gauge location.

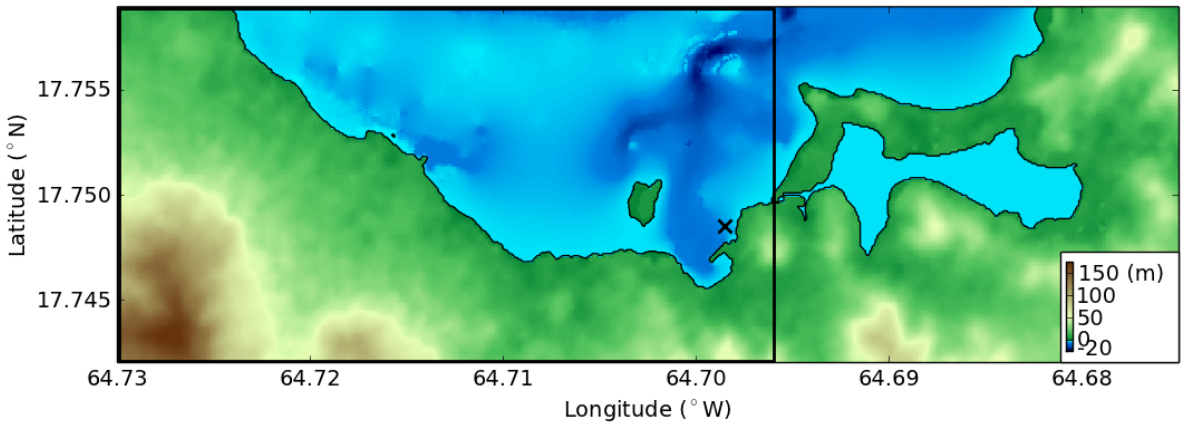

Figure 9: Reference C grid. The contour of optimized C grid is plot in black. The tide gauge location is indicated by the black $\times$.

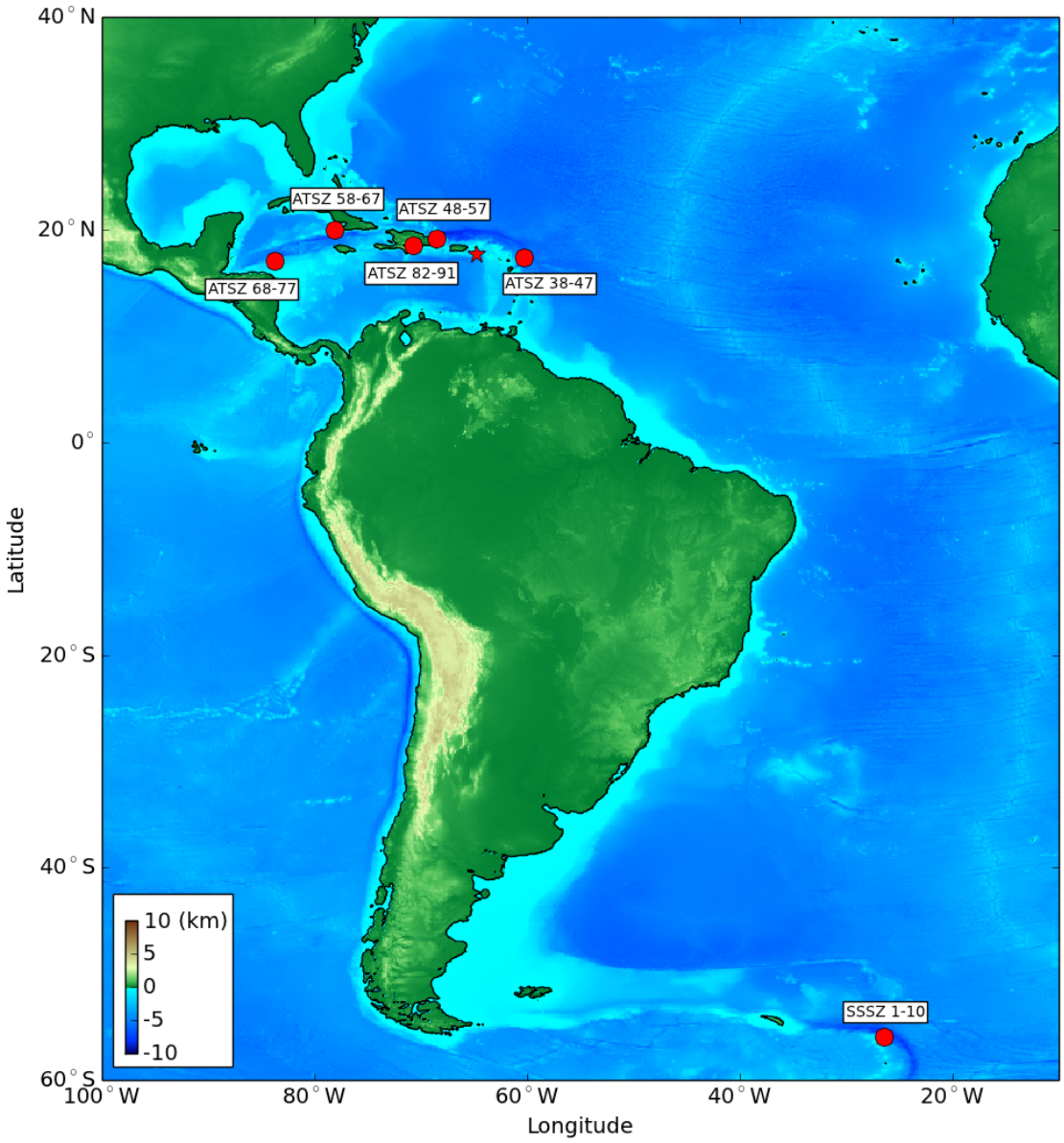

Figure 10: Origins of synthetic mega-tsunami events. The red star denotes the location of Christiansted.

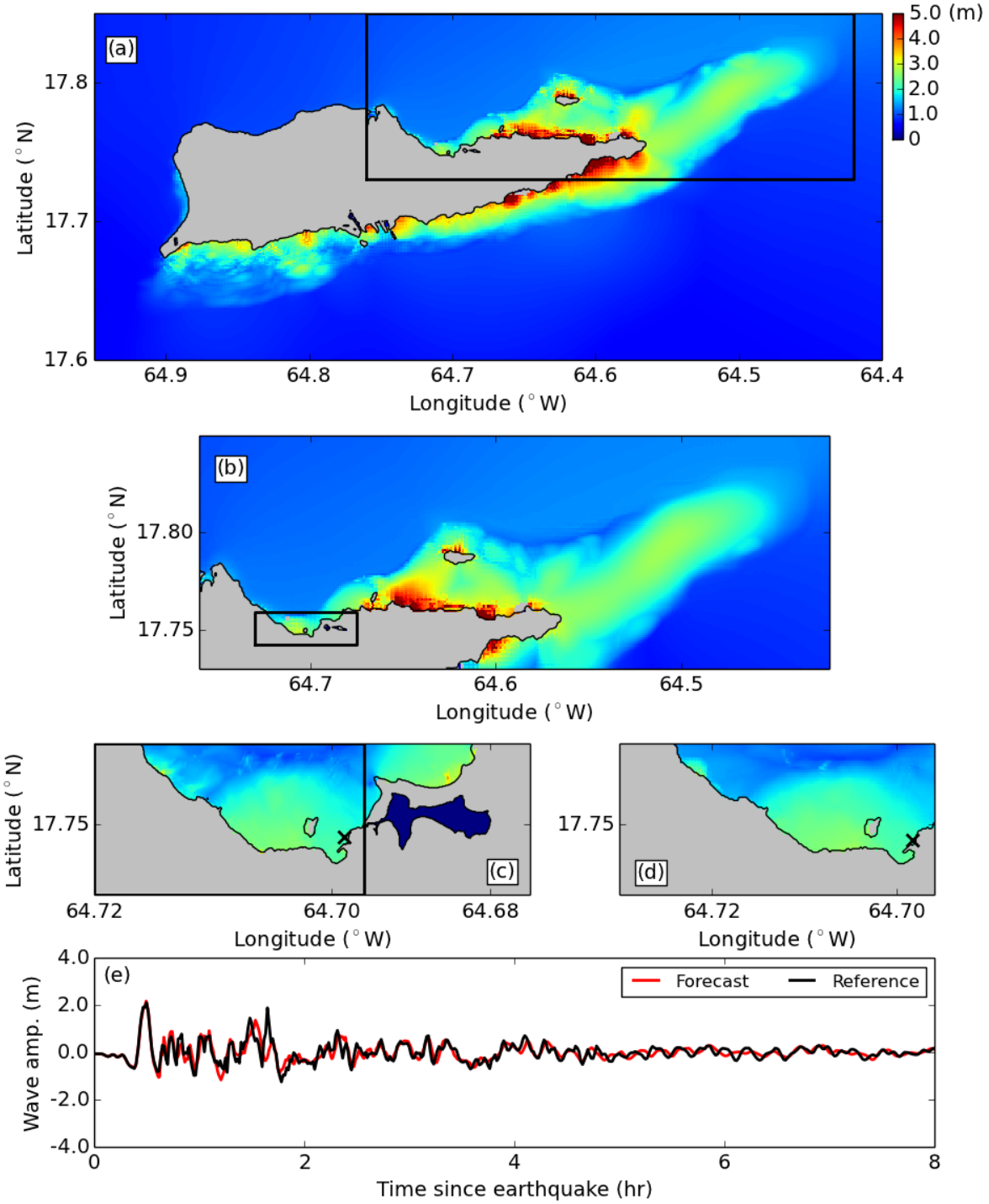

Figure 11: Numerical results for scenario ATSZ 38-47: maximum water surface elevations in reference B grid, with contour of optimized B grid shown in black (a); optimized B grid, with reference C-grid contour shown in black (b); reference C grid, with optimized C-grid contour shown in black (c); optimized C grid (d); and time series of water surface elevations at the reference grid nodes (e). The black × in (c) and (d) indicates gauge location.

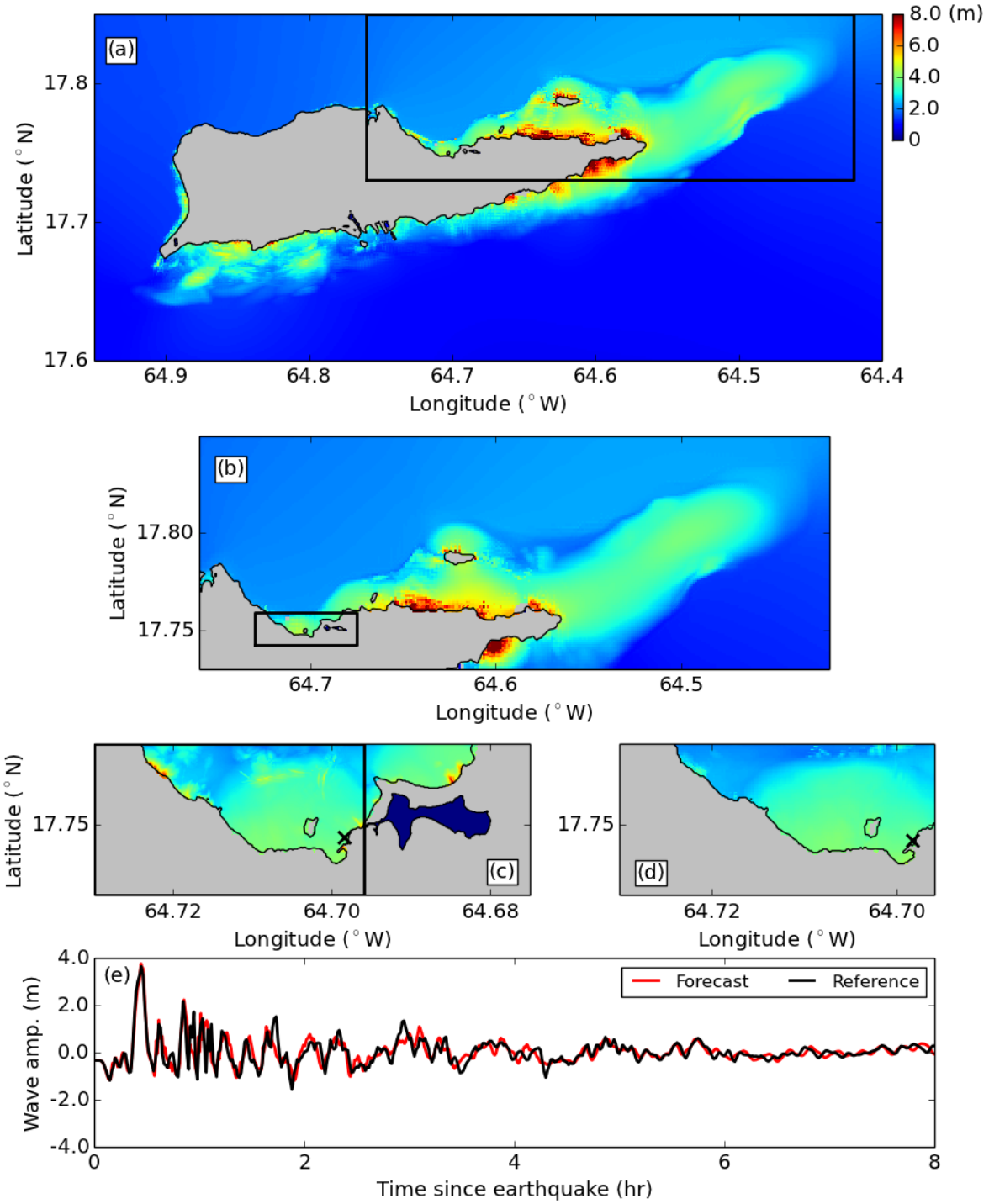

Figure 12: Numerical results for scenario ATSZ 48-57: maximum water surface elevations in reference B grid, with contour of optimized B grid shown in black (a); optimized B grid, with reference C-grid contour shown in black (b); reference C grid, with optimized C-grid contour shown in black (c); optimized C grid (d); and time series of water surface elevations at the reference grid nodes (e). The black × in (c) and (d) indicates gauge location.

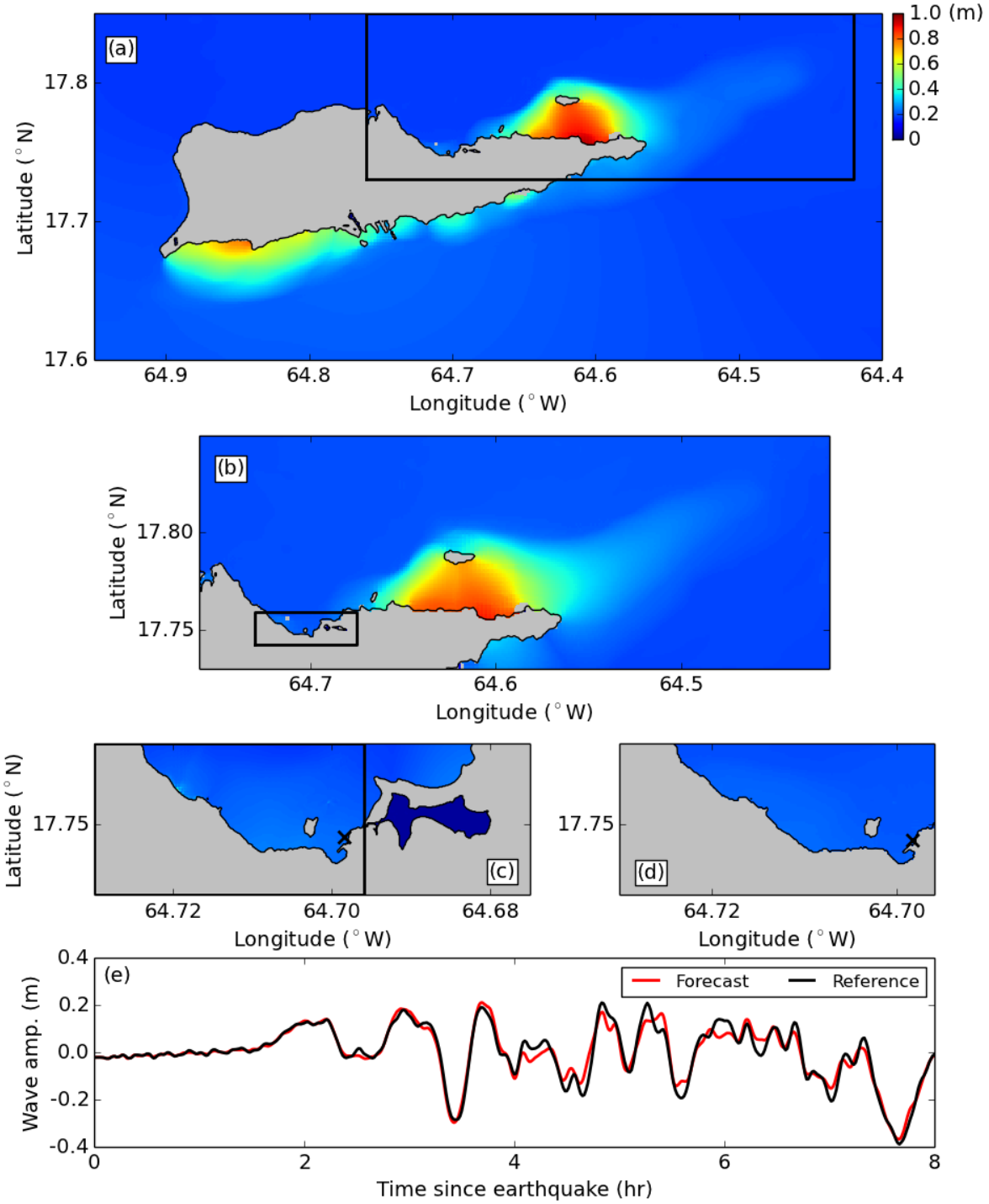

Figure 13: Numerical results for scenario ATSZ 58-67: maximum water surface elevations in reference B grid, with contour of optimized B grid shown in black (a); optimized B grid, with reference C-grid contour shown in black (b); reference C grid, with optimized C-grid contour shown in black (c); optimized C grid (d); and time series of water surface elevations at the reference grid nodes (e). The black × in (c) and (d) indicates gauge location.

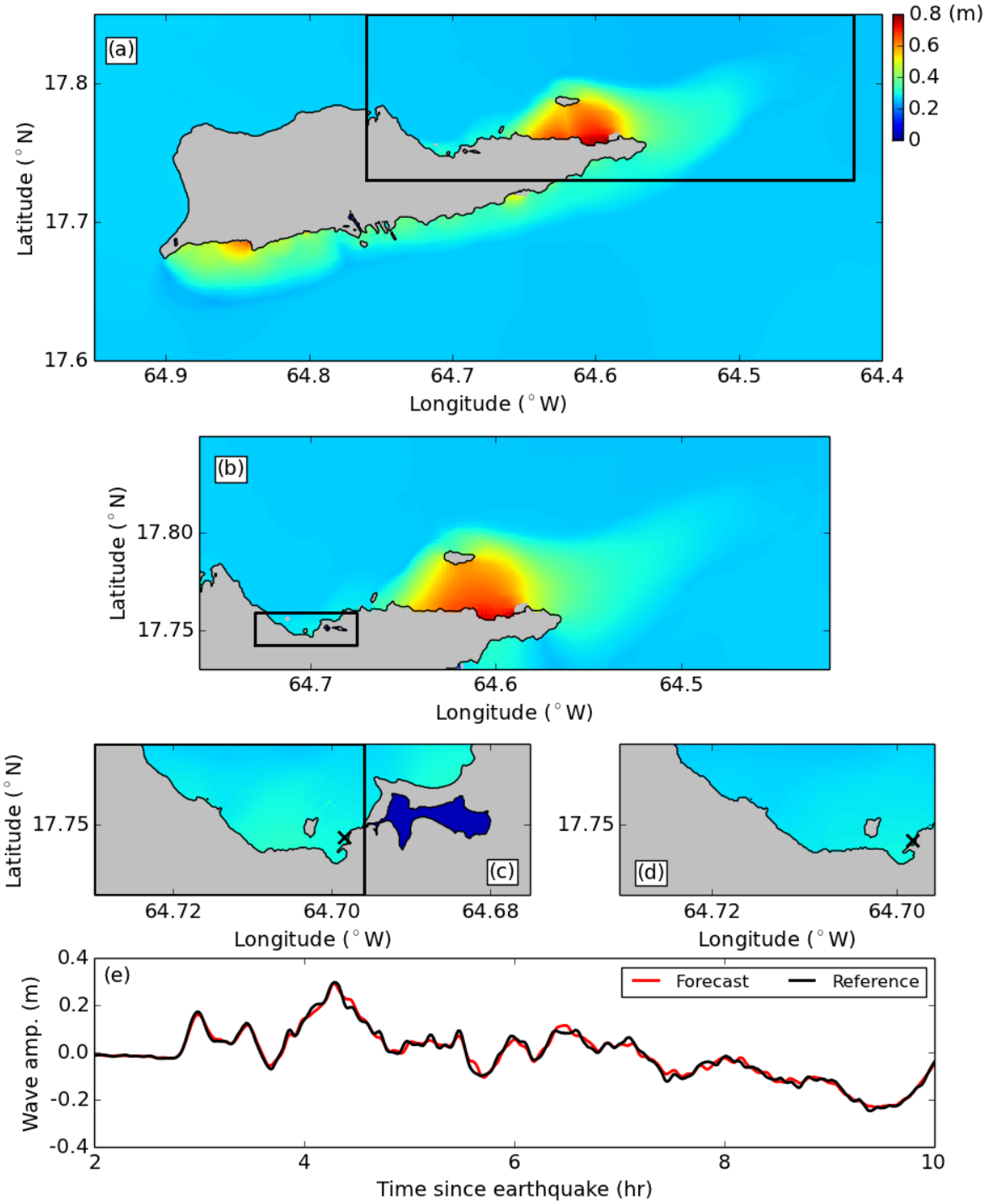

Figure 14: Numerical results for scenario ATSZ 68-77: maximum water surface elevations in reference B grid, with contour of optimized B grid shown in black (a); optimized B grid, with reference C-grid contour shown in black (b); reference C grid, with optimized C-grid contour shown in black (c); optimized C grid (d); and time series of water surface elevations at the reference grid nodes (e). The black × in (c) and (d) indicates gauge location.

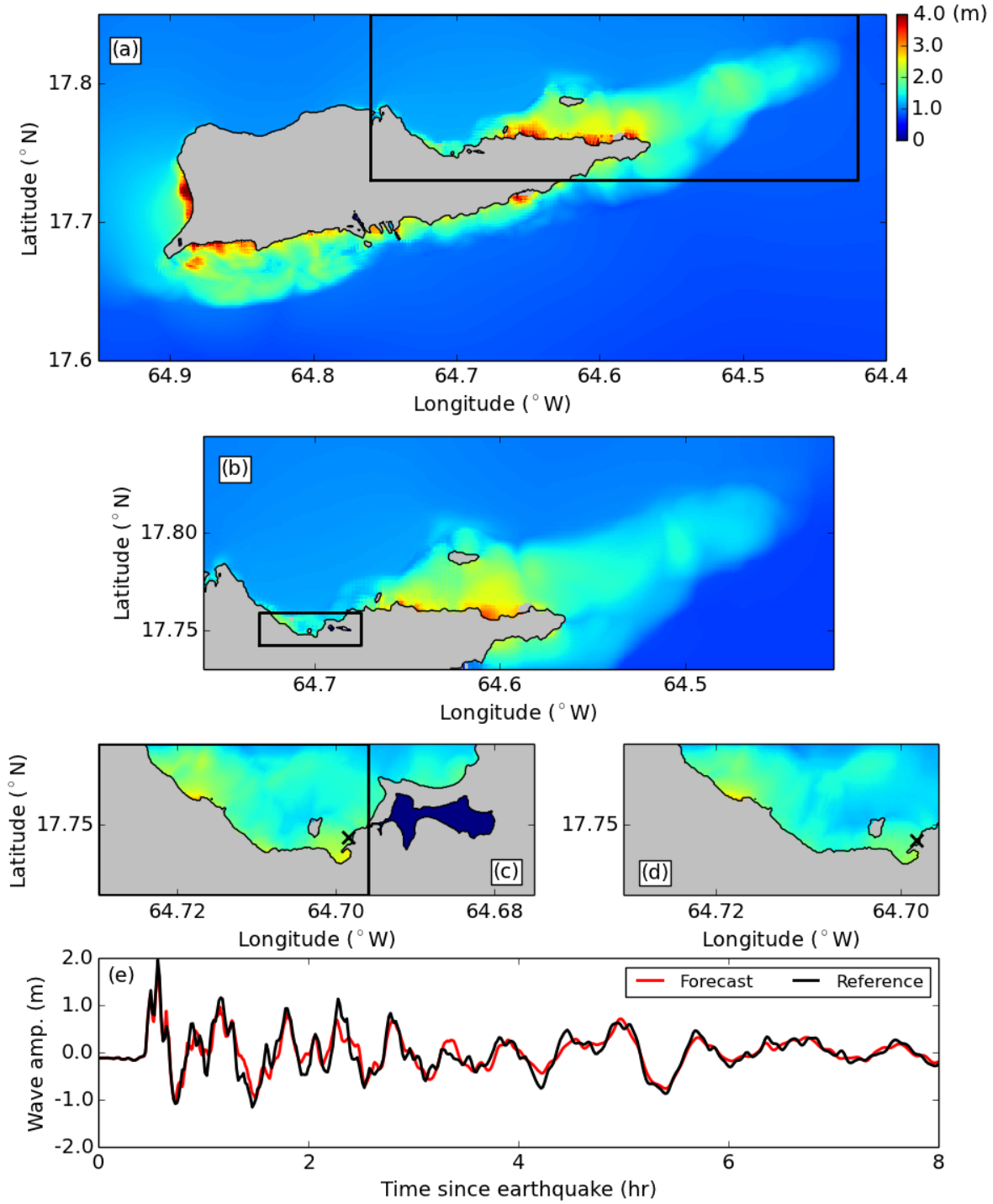

Figure 15: Numerical results for scenario ATSZ 82-91: maximum water surface elevations in reference B grid, with contour of optimized B grid shown in black (a); optimized B grid, with reference C-grid contour shown in black (b); reference C grid, with optimized C-grid contour shown in black (c); optimized C grid (d); and time series of water surface elevations at the reference grid nodes (e). The black × in (c) and (d) indicates gauge location.

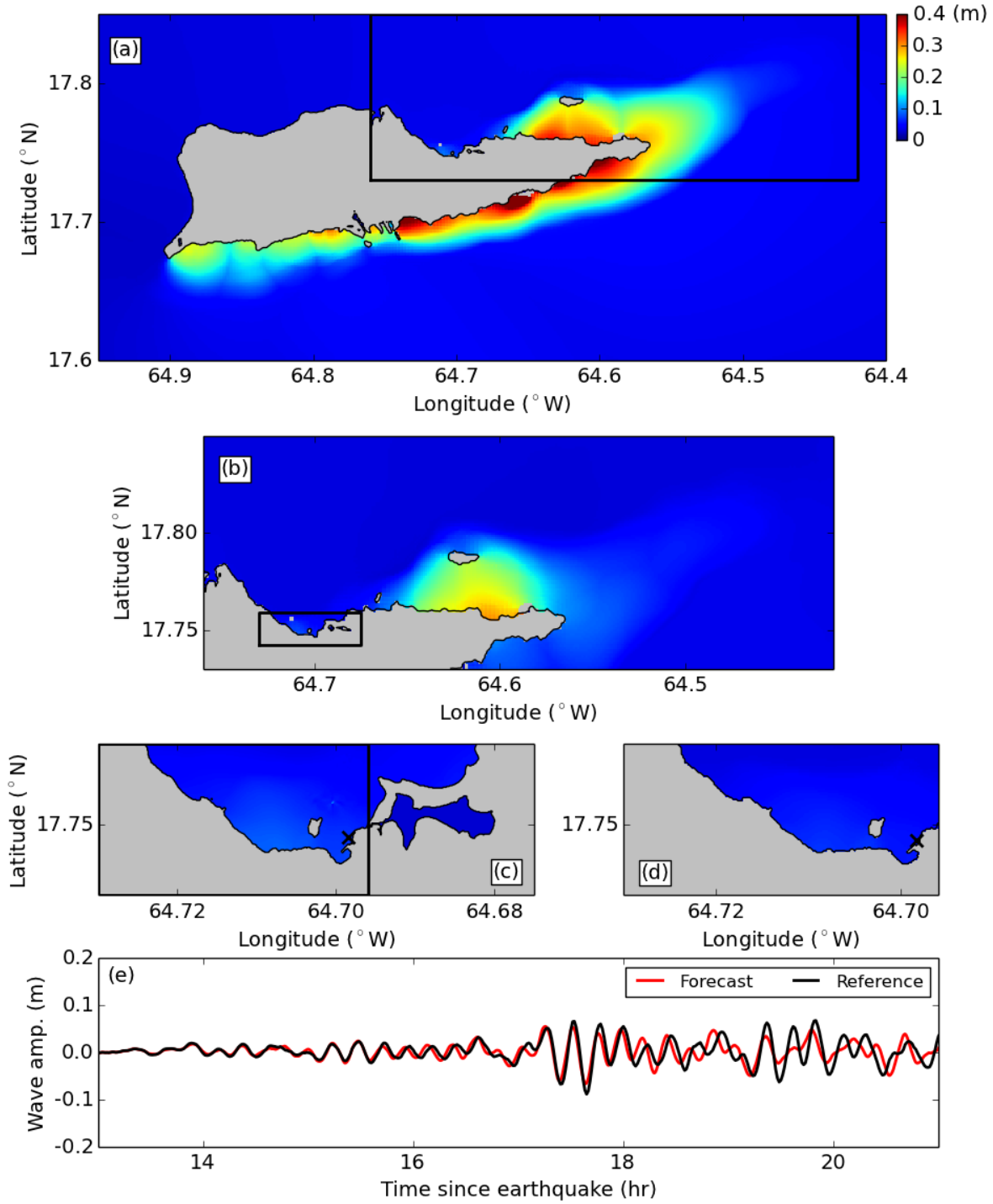

Figure 16: Numerical results for scenario SSSZ 1-10: maximum water surface elevations in reference B grid, with contour of optimized B grid shown in black (a); optimized B grid, with reference C-grid contour shown in black (b); reference C grid, with optimized C-grid contour shown in black (c); optimized C grid (d); and time series of water surface elevations at the reference grid nodes (e). The black × in (c) and (d) indicates gauge location.

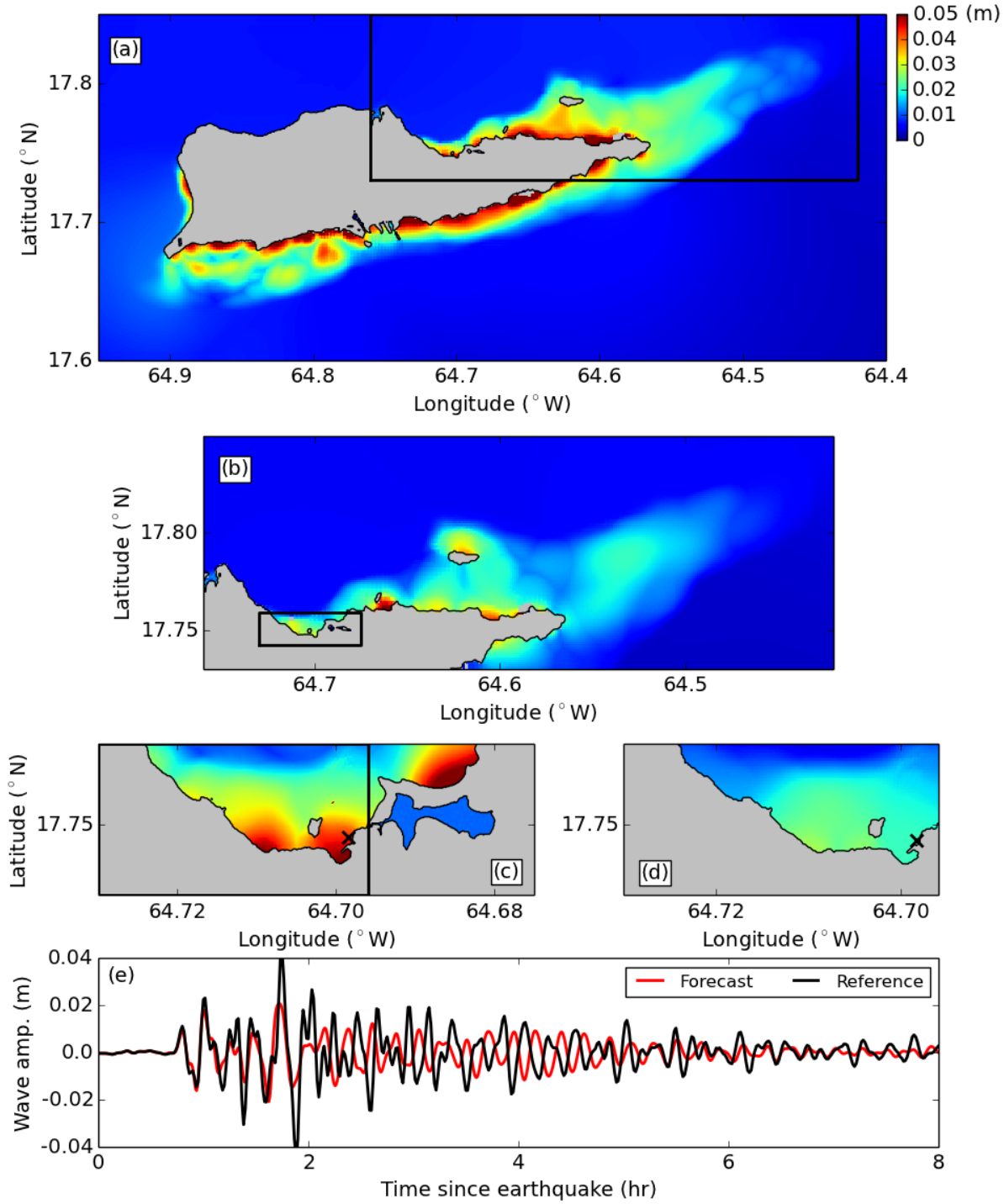

Figure 17: Numerical results for scenario ATSZ B52: maximum water surface elevations in reference B grid, with contour of optimized B grid shown in black (a); optimized B grid, with reference C-grid contour shown in black (b); reference C grid, with optimized C-grid contour shown in black (c); optimized C grid (d); and time series of water surface elevations at the reference grid nodes (e). The black × in (c) and (d) indicates gauge location.

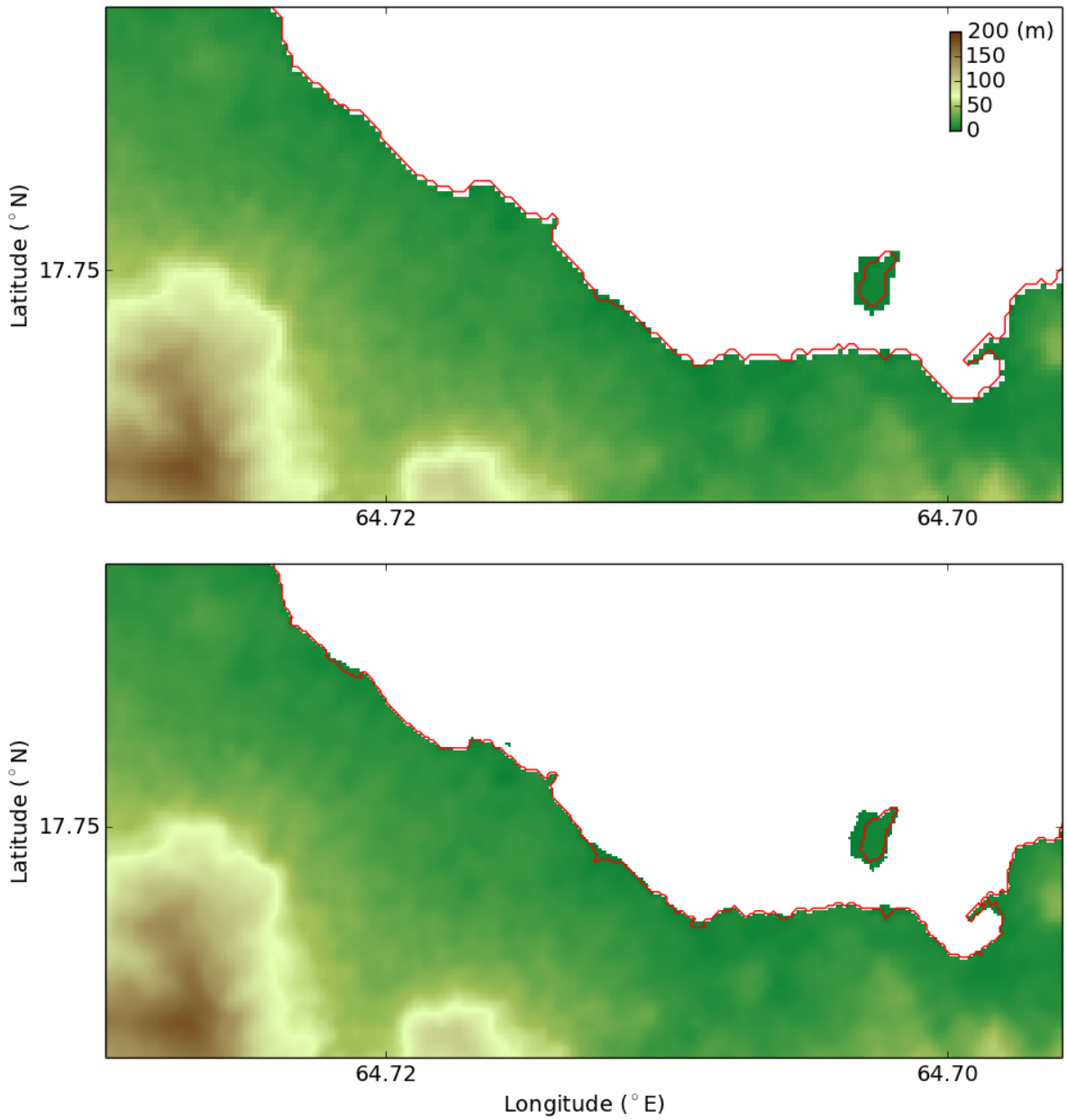

Figure 18: Inundated area in synthetic mega-tsunami event ATSZ 48-57 according to the forecast model (top) and reference model (bottom), respectively. Only originally dry land is shown, with maximum inundation plot as a red line.

Table 1: MOST setup of the reference and forecast models for Christiansted, U.S. Virgin Islands.

		Reference Model				Forecast Model			
Grid	Region	Coverage Lat. (°N) Lon. (°W)	Cell Size Lat. Lon.	nx×ny	Time Step (sec.)	Coverage Lat. (°N) Lon. (°W)	Cell Size Lat. Lon.	nx×ny	Time Step (sec.)
A	Caribbean	16.05–18.95	20″	1612×522	1.5	16.50–18.95	44.8″	610×197	4.8
	Sea	69.90–60.504	21″			69.0–61.0081	47.2″		
B	St. Croix	17.6–17.85	4″	494×224	0.5	17.73–17.85	4″	307×108	0.6
	Island	64.95–64.4	4″			64.76–64.42	4″		
C	Christiansted	17.742–17.759	1/3″	593× 183	0.5	17.742–17.759	2/3″	185×92	0.6
		64.73–64.675	1/3″			64.73–64.696	2/3″		
Minimum offshore depth (m)					1.0				1.0
Water depth for dry land (m)					0.1				0.1
Friction coefficient (n^2)					0.0009				0.0009
CPU time for a 10-hr simulation					$\sim$ 262 min				$\sim$ 24 min

Table 2: Synthetic tsunami scenarios employed to test the Christiansted, U.S. Virgin Islands reference and forecast models.

Scenorio No.	Scenario Name	Source Zone	Tsunami Source	α [m]
Mega-tsunami Scenario				
1	ATSZ 38-47	Atlantic	A38-A47, B38-B47	25
2	ATSZ 48-57	Atlantic	A48-A57, B48-B57	25
3	ATSZ 58-67	Atlantic	A58-A67, B58-B67	25
4	ATSZ 68-77	Atlantic	A68-A77, B68-B77	25
5	ATSZ 82-91	Atlantic	A82-A91, B82-B91	25
6	SSSZ 1-10	South Sandwich	A1-A10, B1-B10	25
Unit-tsunami Scenario				
7	ATSZ B52	Atlantic	B52	1
Micro-tsunami Scenario				
8	SSSZ B11	South Sandwich	B11	0.01

A Model *.in files for Christiansted, U.S. Virgin Islands

A.1 Reference model *.in file

0.01	Minimum amp. of input offshore wave (m)
1.0	Minimum depth of offshore (m)
0.1	Dry land depth of inundation (m)
0.0009	Friction coefficient (n**2)
1	run up in a and b
300.0	max wave height meters
0.5	time step (sec)
72000	number of steps for 10 h simulation
3	Compute "A" arrays every n-th time step, n=
1	Compute "B" arrays every n-th time step, n=
120	Input number of steps between snapshots
0	...starting from
1	...saving grid every n-th node, n=

A.2 Forecast model *.in file

0.01	Minimum amp. of input offshore wave (m)
1.0	Minimum depth of offshore (m)
0.1	Dry land depth of inundation (m)
0.0009	Friction coefficient (n**2)
1	run up in a and b
300.0	max wave height meters
0.6	time step (sec)
60000	number of steps for 10 h simulation
8	Compute "A" arrays every n-th time step, n=
1	Compute "B" arrays every n-th time step, n=
48	Input number of steps between snapshots
0	...starting from
1	...saving grid every n-th node, n=

B Propagation Database: Atlantic Ocean Unit Sources

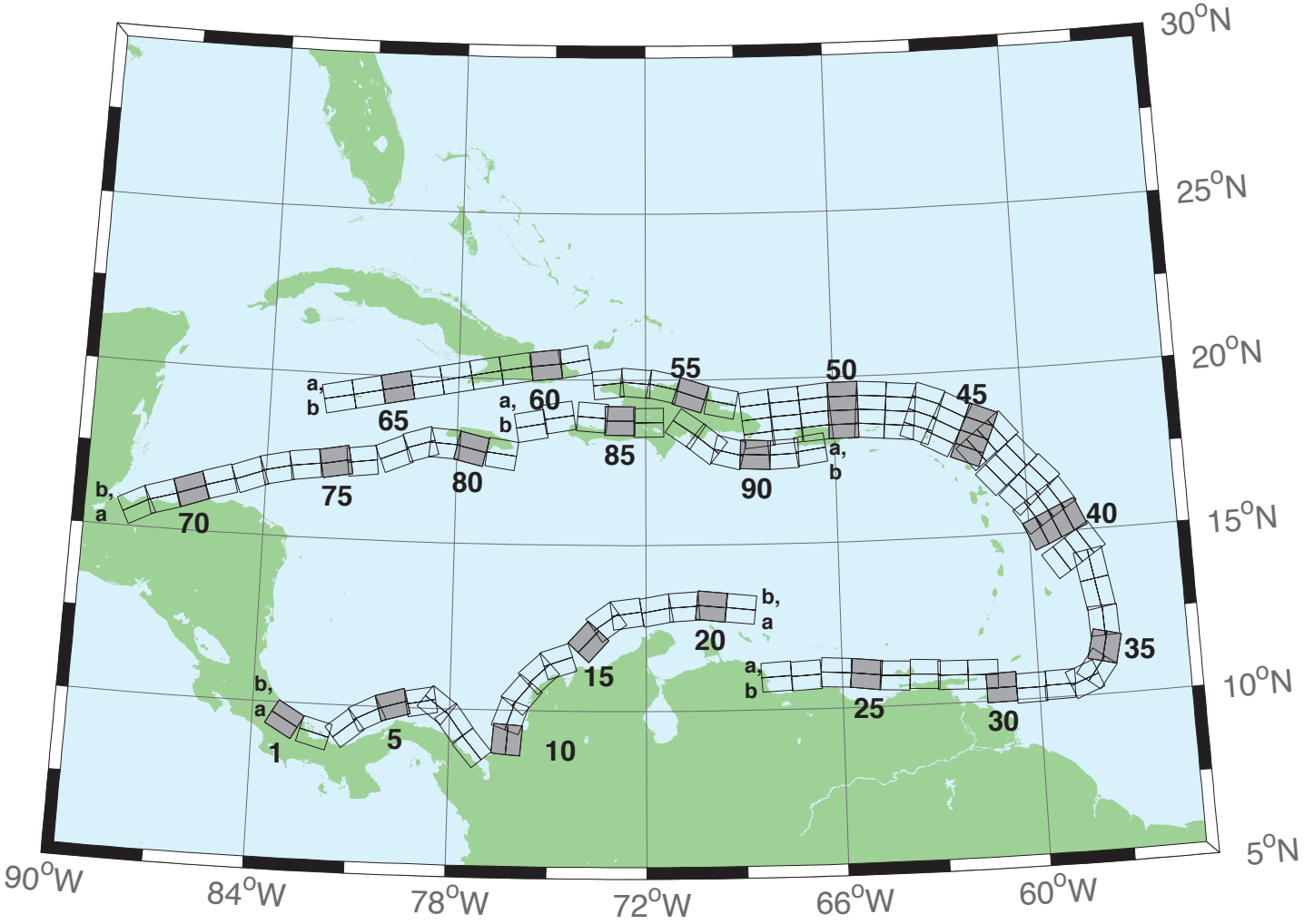

Figure B1: Atlantic Source Zone unit sources.

Table B1: Earthquake parameters for Atlantic Source Zone unit sources.

Segment	Description	Longitude(°E)	Latitude(°N)	Strike(°)	Dip(°)	Depth (km)
atsz–1a	Atlantic Source Zone	-83.2020	9.1449	120	27.5	28.09
atsz–1b	Atlantic Source Zone	-83.0000	9.4899	120	27.5	5
atsz–2a	Atlantic Source Zone	-82.1932	8.7408	105.1	27.5	28.09
atsz–2b	Atlantic Source Zone	-82.0880	9.1254	105.1	27.5	5
atsz–3a	Atlantic Source Zone	-80.9172	9.0103	51.31	30	30
atsz–3b	Atlantic Source Zone	-81.1636	9.3139	51.31	30	5
atsz–4a	Atlantic Source Zone	-80.3265	9.4308	63.49	30	30
atsz–4b	Atlantic Source Zone	-80.5027	9.7789	63.49	30	5
atsz–5a	Atlantic Source Zone	-79.6247	9.6961	74.44	30	30
atsz–5b	Atlantic Source Zone	-79.7307	10.0708	74.44	30	5
atsz–6a	Atlantic Source Zone	-78.8069	9.8083	79.71	30	30
atsz–6b	Atlantic Source Zone	-78.8775	10.1910	79.71	30	5
atsz–7a	Atlantic Source Zone	-78.6237	9.7963	127.2	30	30
atsz–7b	Atlantic Source Zone	-78.3845	10.1059	127.2	30	5
atsz–8a	Atlantic Source Zone	-78.1693	9.3544	143.8	30	30
atsz–8b	Atlantic Source Zone	-77.8511	9.5844	143.8	30	5
atsz–9a	Atlantic Source Zone	-77.5913	8.5989	139.9	30	30
atsz–9b	Atlantic Source Zone	-77.2900	8.8493	139.9	30	5
atsz–10a	Atlantic Source Zone	-75.8109	9.0881	4.67	17	19.62
atsz–10b	Atlantic Source Zone	-76.2445	9.1231	4.67	17	5
atsz–11a	Atlantic Source Zone	-75.7406	9.6929	19.67	17	19.62
atsz–11b	Atlantic Source Zone	-76.1511	9.8375	19.67	17	5
atsz–12a	Atlantic Source Zone	-75.4763	10.2042	40.4	17	19.62
atsz–12b	Atlantic Source Zone	-75.8089	10.4826	40.4	17	5
atsz–13a	Atlantic Source Zone	-74.9914	10.7914	47.17	17	19.62
atsz–13b	Atlantic Source Zone	-75.2890	11.1064	47.17	17	5
atsz–14a	Atlantic Source Zone	-74.5666	11.0708	71.68	17	19.62
atsz–14b	Atlantic Source Zone	-74.7043	11.4786	71.68	17	5
atsz–15a	Atlantic Source Zone	-73.4576	11.8012	42.69	17	19.62
atsz–15b	Atlantic Source Zone	-73.7805	12.0924	42.69	17	5
atsz–16a	Atlantic Source Zone	-72.9788	12.3365	54.75	17	19.62
atsz–16b	Atlantic Source Zone	-73.2329	12.6873	54.75	17	5
atsz–17a	Atlantic Source Zone	-72.5454	12.5061	81.96	17	19.62
atsz–17b	Atlantic Source Zone	-72.6071	12.9314	81.96	17	5
atsz–18a	Atlantic Source Zone	-71.6045	12.6174	79.63	17	19.62
atsz–18b	Atlantic Source Zone	-71.6839	13.0399	79.63	17	5
atsz–19a	Atlantic Source Zone	-70.7970	12.7078	86.32	17	19.62
atsz–19b	Atlantic Source Zone	-70.8253	13.1364	86.32	17	5
atsz–20a	Atlantic Source Zone	-70.0246	12.7185	95.94	17	19.62
atsz–20b	Atlantic Source Zone	-69.9789	13.1457	95.94	17	5
atsz–21a	Atlantic Source Zone	-69.1244	12.6320	95.94	17	19.62
atsz–21b	Atlantic Source Zone	-69.0788	13.0592	95.94	17	5
atsz–22a	Atlantic Source Zone	-68.0338	11.4286	266.9	15	17.94
atsz–22b	Atlantic Source Zone	-68.0102	10.9954	266.9	15	5
atsz–23a	Atlantic Source Zone	-67.1246	11.4487	266.9	15	17.94
atsz–23b	Atlantic Source Zone	-67.1010	11.0155	266.9	15	5
atsz–24a	Atlantic Source Zone	-66.1656	11.5055	273.3	15	17.94
atsz–24b	Atlantic Source Zone	-66.1911	11.0724	273.3	15	5
atsz–25a	Atlantic Source Zone	-65.2126	11.4246	276.4	15	17.94
atsz–25b	Atlantic Source Zone	-65.2616	10.9934	276.4	15	5
atsz–26a	Atlantic Source Zone	-64.3641	11.3516	272.9	15	17.94
atsz–26b	Atlantic Source Zone	-64.3862	10.9183	272.9	15	5
atsz–27a	Atlantic Source Zone	-63.4472	11.3516	272.9	15	17.94
atsz–27b	Atlantic Source Zone	-63.4698	10.9183	272.9	15	5
atsz–28a	Atlantic Source Zone	-62.6104	11.2831	271.1	15	17.94
atsz–28b	Atlantic Source Zone	-62.6189	10.8493	271.1	15	5
atsz–29a	Atlantic Source Zone	-61.6826	11.2518	271.6	15	17.94
atsz–29b	Atlantic Source Zone	-61.6947	10.8181	271.6	15	5
atsz–30a	Atlantic Source Zone	-61.1569	10.8303	269	15	17.94
atsz–30b	Atlantic Source Zone	-61.1493	10.3965	269	15	5
atsz–31a	Atlantic Source Zone	-60.2529	10.7739	269	15	17.94
atsz–31b	Atlantic Source Zone	-60.2453	10.3401	269	15	5
atsz–32a	Atlantic Source Zone	-59.3510	10.8123	269	15	17.94

Continued on next page

Table B1 – continued from previous page

Segment	Description	Longitude(°E)	Latitude(°N)	Strike(°)	Dip(°)	Depth (km)
atsz–32b	Atlantic Source Zone	-59.3734	10.3785	269	15	5
atsz–33a	Atlantic Source Zone	-58.7592	10.8785	248.6	15	17.94
atsz–33b	Atlantic Source Zone	-58.5984	10.4745	248.6	15	5
atsz–34a	Atlantic Source Zone	-58.5699	11.0330	217.2	15	17.94
atsz–34b	Atlantic Source Zone	-58.2179	10.7710	217.2	15	5
atsz–35a	Atlantic Source Zone	-58.3549	11.5300	193.7	15	17.94
atsz–35b	Atlantic Source Zone	-57.9248	11.4274	193.7	15	5
atsz–36a	Atlantic Source Zone	-58.3432	12.1858	177.7	15	17.94
atsz–36b	Atlantic Source Zone	-57.8997	12.2036	177.7	15	5
atsz–37a	Atlantic Source Zone	-58.4490	12.9725	170.7	15	17.94
atsz–37b	Atlantic Source Zone	-58.0095	13.0424	170.7	15	5
atsz–38a	Atlantic Source Zone	-58.6079	13.8503	170.2	15	17.94
atsz–38b	Atlantic Source Zone	-58.1674	13.9240	170.2	15	5
atsz–39a	Atlantic Source Zone	-58.6667	14.3915	146.8	15	17.94
atsz–39b	Atlantic Source Zone	-58.2913	14.6287	146.8	15	5
atsz–39y	Atlantic Source Zone	-59.4168	13.9171	146.8	15	43.82
atsz–39z	Atlantic Source Zone	-59.0415	14.1543	146.8	15	30.88
atsz–40a	Atlantic Source Zone	-59.1899	15.2143	156.2	15	17.94
atsz–40b	Atlantic Source Zone	-58.7781	15.3892	156.2	15	5
atsz–40y	Atlantic Source Zone	-60.0131	14.8646	156.2	15	43.82
atsz–40z	Atlantic Source Zone	-59.6012	15.0395	156.2	15	30.88
atsz–41a	Atlantic Source Zone	-59.4723	15.7987	146.3	15	17.94
atsz–41b	Atlantic Source Zone	-59.0966	16.0392	146.3	15	5
atsz–41y	Atlantic Source Zone	-60.2229	15.3177	146.3	15	43.82
atsz–41z	Atlantic Source Zone	-59.8473	15.5582	146.3	15	30.88
atsz–42a	Atlantic Source Zone	-59.9029	16.4535	137	15	17.94
atsz–42b	Atlantic Source Zone	-59.5716	16.7494	137	15	5
atsz–42y	Atlantic Source Zone	-60.5645	15.8616	137	15	43.82
atsz–42z	Atlantic Source Zone	-60.2334	16.1575	137	15	30.88
atsz–43a	Atlantic Source Zone	-60.5996	17.0903	138.7	15	17.94
atsz–43b	Atlantic Source Zone	-60.2580	17.3766	138.7	15	5
atsz–43y	Atlantic Source Zone	-61.2818	16.5177	138.7	15	43.82
atsz–43z	Atlantic Source Zone	-60.9404	16.8040	138.7	15	30.88
atsz–44a	Atlantic Source Zone	-61.1559	17.8560	141.1	15	17.94
atsz–44b	Atlantic Source Zone	-60.8008	18.1286	141.1	15	5
atsz–44y	Atlantic Source Zone	-61.8651	17.3108	141.1	15	43.82
atsz–44z	Atlantic Source Zone	-61.5102	17.5834	141.1	15	30.88
atsz–45a	Atlantic Source Zone	-61.5491	18.0566	112.8	15	17.94
atsz–45b	Atlantic Source Zone	-61.3716	18.4564	112.8	15	5
atsz–45y	Atlantic Source Zone	-61.9037	17.2569	112.8	15	43.82
atsz–45z	Atlantic Source Zone	-61.7260	17.6567	112.8	15	30.88
atsz–46a	Atlantic Source Zone	-62.4217	18.4149	117.9	15	17.94
atsz–46b	Atlantic Source Zone	-62.2075	18.7985	117.9	15	5
atsz–46y	Atlantic Source Zone	-62.8493	17.6477	117.9	15	43.82
atsz–46z	Atlantic Source Zone	-62.6352	18.0313	117.9	15	30.88
atsz–47a	Atlantic Source Zone	-63.1649	18.7844	110.5	20	22.1
atsz–47b	Atlantic Source Zone	-63.0087	19.1798	110.5	20	5
atsz–47y	Atlantic Source Zone	-63.4770	17.9936	110.5	20	56.3
atsz–47z	Atlantic Source Zone	-63.3205	18.3890	110.5	20	39.2
atsz–48a	Atlantic Source Zone	-63.8800	18.8870	95.37	20	22.1
atsz–48b	Atlantic Source Zone	-63.8382	19.3072	95.37	20	5
atsz–48y	Atlantic Source Zone	-63.9643	18.0465	95.37	20	56.3
atsz–48z	Atlantic Source Zone	-63.9216	18.4667	95.37	20	39.2
atsz–49a	Atlantic Source Zone	-64.8153	18.9650	94.34	20	22.1
atsz–49b	Atlantic Source Zone	-64.7814	19.3859	94.34	20	5
atsz–49y	Atlantic Source Zone	-64.8840	18.1233	94.34	20	56.3
atsz–49z	Atlantic Source Zone	-64.8492	18.5442	94.34	20	39.2
atsz–50a	Atlantic Source Zone	-65.6921	18.9848	89.59	20	22.1
atsz–50b	Atlantic Source Zone	-65.6953	19.4069	89.59	20	5
atsz–50y	Atlantic Source Zone	-65.6874	18.1407	89.59	20	56.3
atsz–50z	Atlantic Source Zone	-65.6887	18.5628	89.59	20	39.2
atsz–51a	Atlantic Source Zone	-66.5742	18.9484	84.98	20	22.1
atsz–51b	Atlantic Source Zone	-66.6133	19.3688	84.98	20	5
atsz–51y	Atlantic Source Zone	-66.4977	18.1076	84.98	20	56.3

Continued on next page

Table B1 – continued from previous page

Segment	Description	Longitude(°E)	Latitude(°N)	Strike(°)	Dip(°)	Depth (km)
atsz–51z	Atlantic Source Zone	-66.5353	18.5280	84.98	20	39.2
atsz–52a	Atlantic Source Zone	-67.5412	18.8738	85.87	20	22.1
atsz–52b	Atlantic Source Zone	-67.5734	19.2948	85.87	20	5
atsz–52y	Atlantic Source Zone	-67.4781	18.0319	85.87	20	56.3
atsz–52z	Atlantic Source Zone	-67.5090	18.4529	85.87	20	39.2
atsz–53a	Atlantic Source Zone	-68.4547	18.7853	83.64	20	22.1
atsz–53b	Atlantic Source Zone	-68.5042	19.2048	83.64	20	5
atsz–53y	Atlantic Source Zone	-68.3575	17.9463	83.64	20	56.3
atsz–53z	Atlantic Source Zone	-68.4055	18.3658	83.64	20	39.2
atsz–54a	Atlantic Source Zone	-69.6740	18.8841	101.5	20	22.1
atsz–54b	Atlantic Source Zone	-69.5846	19.2976	101.5	20	5
atsz–55a	Atlantic Source Zone	-70.7045	19.1376	108.2	20	22.1
atsz–55b	Atlantic Source Zone	-70.5647	19.5386	108.2	20	5
atsz–56a	Atlantic Source Zone	-71.5368	19.3853	102.6	20	22.1
atsz–56b	Atlantic Source Zone	-71.4386	19.7971	102.6	20	5
atsz–57a	Atlantic Source Zone	-72.3535	19.4838	94.2	20	22.1
atsz–57b	Atlantic Source Zone	-72.3206	19.9047	94.2	20	5
atsz–58a	Atlantic Source Zone	-73.1580	19.4498	84.34	20	22.1
atsz–58b	Atlantic Source Zone	-73.2022	19.8698	84.34	20	5
atsz–59a	Atlantic Source Zone	-74.3567	20.9620	259.7	20	22.1
atsz–59b	Atlantic Source Zone	-74.2764	20.5467	259.7	20	5
atsz–60a	Atlantic Source Zone	-75.2386	20.8622	264.2	15	17.94
atsz–60b	Atlantic Source Zone	-75.1917	20.4306	264.2	15	5
atsz–61a	Atlantic Source Zone	-76.2383	20.7425	260.7	15	17.94
atsz–61b	Atlantic Source Zone	-76.1635	20.3144	260.7	15	5
atsz–62a	Atlantic Source Zone	-77.2021	20.5910	259.9	15	17.94
atsz–62b	Atlantic Source Zone	-77.1214	20.1638	259.9	15	5
atsz–63a	Atlantic Source Zone	-78.1540	20.4189	259	15	17.94
atsz–63b	Atlantic Source Zone	-78.0661	19.9930	259	15	5
atsz–64a	Atlantic Source Zone	-79.0959	20.2498	259.2	15	17.94
atsz–64b	Atlantic Source Zone	-79.0098	19.8236	259.2	15	5
atsz–65a	Atlantic Source Zone	-80.0393	20.0773	258.9	15	17.94
atsz–65b	Atlantic Source Zone	-79.9502	19.6516	258.9	15	5
atsz–66a	Atlantic Source Zone	-80.9675	19.8993	258.6	15	17.94
atsz–66b	Atlantic Source Zone	-80.8766	19.4740	258.6	15	5
atsz–67a	Atlantic Source Zone	-81.9065	19.7214	258.5	15	17.94
atsz–67b	Atlantic Source Zone	-81.8149	19.2962	258.5	15	5
atsz–68a	Atlantic Source Zone	-87.8003	15.2509	62.69	15	17.94
atsz–68b	Atlantic Source Zone	-88.0070	15.6364	62.69	15	5
atsz–69a	Atlantic Source Zone	-87.0824	15.5331	72.73	15	17.94
atsz–69b	Atlantic Source Zone	-87.2163	15.9474	72.73	15	5
atsz–70a	Atlantic Source Zone	-86.1622	15.8274	70.64	15	17.94
atsz–70b	Atlantic Source Zone	-86.3120	16.2367	70.64	15	5
atsz–71a	Atlantic Source Zone	-85.3117	16.1052	73.7	15	17.94
atsz–71b	Atlantic Source Zone	-85.4387	16.5216	73.7	15	5
atsz–72a	Atlantic Source Zone	-84.3470	16.3820	69.66	15	17.94
atsz–72b	Atlantic Source Zone	-84.5045	16.7888	69.66	15	5
atsz–73a	Atlantic Source Zone	-83.5657	16.6196	77.36	15	17.94
atsz–73b	Atlantic Source Zone	-83.6650	17.0429	77.36	15	5
atsz–74a	Atlantic Source Zone	-82.7104	16.7695	82.35	15	17.94
atsz–74b	Atlantic Source Zone	-82.7709	17.1995	82.35	15	5
atsz–75a	Atlantic Source Zone	-81.7297	16.9003	79.86	15	17.94
atsz–75b	Atlantic Source Zone	-81.8097	17.3274	79.86	15	5
atsz–76a	Atlantic Source Zone	-80.9196	16.9495	82.95	15	17.94
atsz–76b	Atlantic Source Zone	-80.9754	17.3801	82.95	15	5
atsz–77a	Atlantic Source Zone	-79.8086	17.2357	67.95	15	17.94
atsz–77b	Atlantic Source Zone	-79.9795	17.6378	67.95	15	5
atsz–78a	Atlantic Source Zone	-79.0245	17.5415	73.61	15	17.94
atsz–78b	Atlantic Source Zone	-79.1532	17.9577	73.61	15	5
atsz–79a	Atlantic Source Zone	-78.4122	17.5689	94.07	15	17.94
atsz–79b	Atlantic Source Zone	-78.3798	18.0017	94.07	15	5
atsz–80a	Atlantic Source Zone	-77.6403	17.4391	103.3	15	17.94
atsz–80b	Atlantic Source Zone	-77.5352	17.8613	103.3	15	5
atsz–81a	Atlantic Source Zone	-76.6376	17.2984	98.21	15	17.94

Continued on next page

Table B1 – continued from previous page

Segment	Description	Longitude(°E)	Latitude(°N)	Strike(°)	Dip(°)	Depth (km)
atsz–81b	Atlantic Source Zone	-76.5726	17.7278	98.21	15	5
atsz–82a	Atlantic Source Zone	-75.7299	19.0217	260.1	15	17.94
atsz–82b	Atlantic Source Zone	-75.6516	18.5942	260.1	15	5
atsz–83a	Atlantic Source Zone	-74.8351	19.2911	260.8	15	17.94
atsz–83b	Atlantic Source Zone	-74.7621	18.8628	260.8	15	5
atsz–84a	Atlantic Source Zone	-73.6639	19.2991	274.8	15	17.94
atsz–84b	Atlantic Source Zone	-73.7026	18.8668	274.8	15	5
atsz–85a	Atlantic Source Zone	-72.8198	19.2019	270.6	15	17.94
atsz–85b	Atlantic Source Zone	-72.8246	18.7681	270.6	15	5
atsz–86a	Atlantic Source Zone	-71.9143	19.1477	269.1	15	17.94
atsz–86b	Atlantic Source Zone	-71.9068	18.7139	269.1	15	5
atsz–87a	Atlantic Source Zone	-70.4738	18.8821	304.5	15	17.94
atsz–87b	Atlantic Source Zone	-70.7329	18.5245	304.5	15	5
atsz–88a	Atlantic Source Zone	-69.7710	18.3902	308.9	15	17.94
atsz–88b	Atlantic Source Zone	-70.0547	18.0504	308.4	15	5
atsz–89a	Atlantic Source Zone	-69.2635	18.2099	283.9	15	17.94
atsz–89b	Atlantic Source Zone	-69.3728	17.7887	283.9	15	5
atsz–90a	Atlantic Source Zone	-68.5059	18.1443	272.9	15	17.94
atsz–90b	Atlantic Source Zone	-68.5284	17.7110	272.9	15	5
atsz–91a	Atlantic Source Zone	-67.6428	18.1438	267.8	15	17.94
atsz–91b	Atlantic Source Zone	-67.6256	17.7103	267.8	15	5
atsz–92a	Atlantic Source Zone	-66.8261	18.2536	262	15	17.94
atsz–92b	Atlantic Source Zone	-66.7627	17.8240	262	15	5

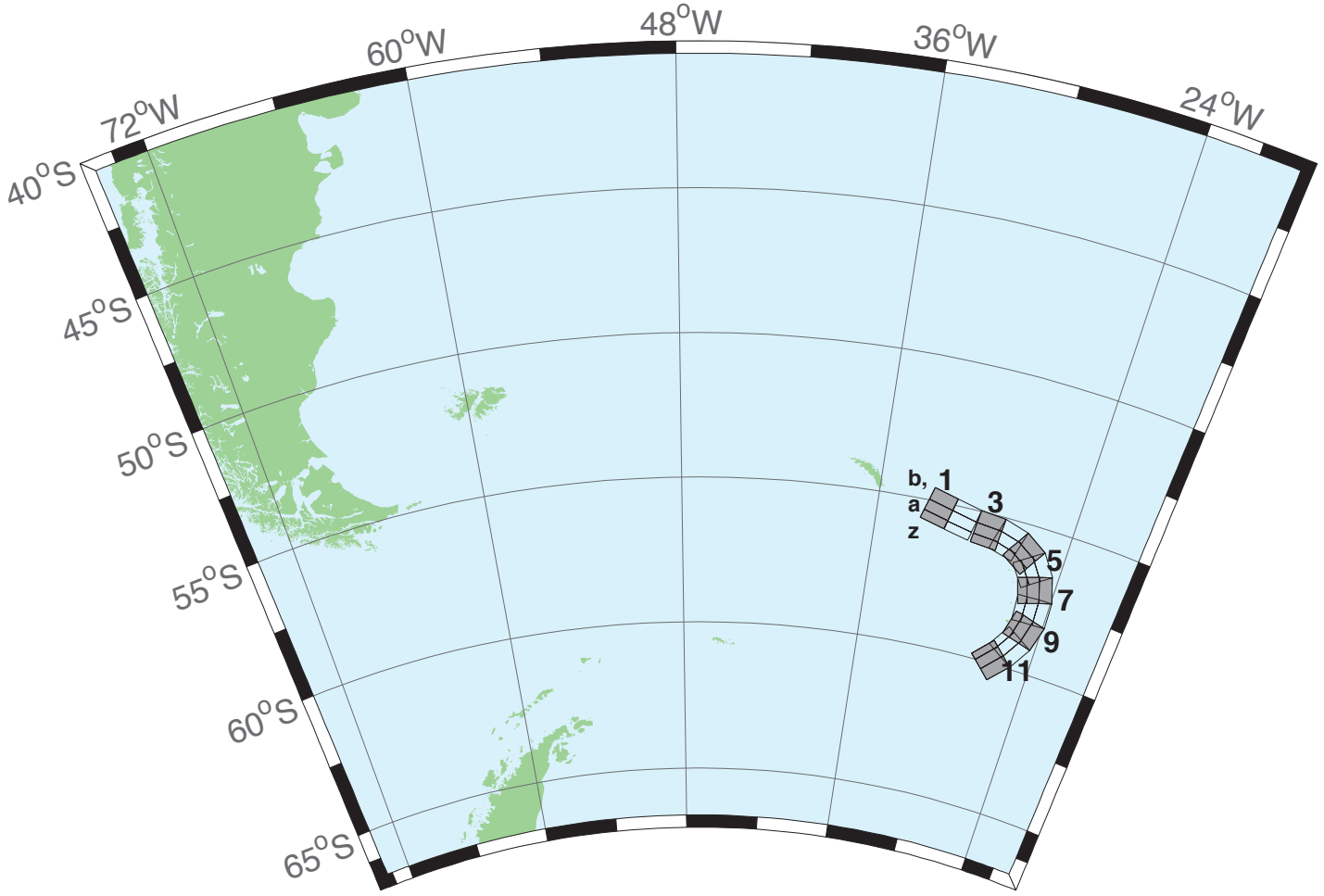

Figure B2: South Sandwich Islands Subduction Zone.

Table B2: Earthquake parameters for South Sandwich Islands Subduction Zone unit sources.

Segment	Description	Longitude(°E)	Latitude(°N)	Strike(°)	Dip(°)	Depth (km)
sssz–1a	South Sandwich Islands Subduction Zone	-32.3713	-55.4655	104.7	28.53	17.51
sssz–1b	South Sandwich Islands Subduction Zone	-32.1953	-55.0832	104.7	9.957	8.866
sssz–1z	South Sandwich Islands Subduction Zone	-32.5091	-55.7624	104.7	46.99	41.39
sssz–2a	South Sandwich Islands Subduction Zone	-30.8028	-55.6842	102.4	28.53	17.51
sssz–2b	South Sandwich Islands Subduction Zone	-30.6524	-55.2982	102.4	9.957	8.866
sssz–2z	South Sandwich Islands Subduction Zone	-30.9206	-55.9839	102.4	46.99	41.39
sssz–3a	South Sandwich Islands Subduction Zone	-29.0824	-55.8403	95.53	28.53	17.51
sssz–3b	South Sandwich Islands Subduction Zone	-29.0149	-55.4468	95.53	9.957	8.866
sssz–3z	South Sandwich Islands Subduction Zone	-29.1353	-56.1458	95.53	46.99	41.39
sssz–4a	South Sandwich Islands Subduction Zone	-27.8128	-55.9796	106.1	28.53	17.51
sssz–4b	South Sandwich Islands Subduction Zone	-27.6174	-55.5999	106.1	9.957	8.866
sssz–4z	South Sandwich Islands Subduction Zone	-27.9659	-56.2744	106.1	46.99	41.39
sssz–5a	South Sandwich Islands Subduction Zone	-26.7928	-56.2481	123.1	28.53	17.51
sssz–5b	South Sandwich Islands Subduction Zone	-26.4059	-55.9170	123.1	9.957	8.866
sssz–5z	South Sandwich Islands Subduction Zone	-27.0955	-56.5052	123.1	46.99	41.39
sssz–6a	South Sandwich Islands Subduction Zone	-26.1317	-56.6466	145.6	23.28	16.11
sssz–6b	South Sandwich Islands Subduction Zone	-25.5131	-56.4133	145.6	9.09	8.228
sssz–6z	South Sandwich Islands Subduction Zone	-26.5920	-56.8194	145.6	47.15	35.87
sssz–7a	South Sandwich Islands Subduction Zone	-25.6787	-57.2162	162.9	21.21	14.23
sssz–7b	South Sandwich Islands Subduction Zone	-24.9394	-57.0932	162.9	7.596	7.626
sssz–7z	South Sandwich Islands Subduction Zone	-26.2493	-57.3109	162.9	44.16	32.32
sssz–8a	South Sandwich Islands Subduction Zone	-25.5161	-57.8712	178.2	20.33	15.91
sssz–8b	South Sandwich Islands Subduction Zone	-24.7233	-57.8580	178.2	8.449	8.562
sssz–8z	South Sandwich Islands Subduction Zone	-26.1280	-57.8813	178.2	43.65	33.28
sssz–9a	South Sandwich Islands Subduction Zone	-25.6657	-58.5053	195.4	25.76	15.71
sssz–9b	South Sandwich Islands Subduction Zone	-24.9168	-58.6127	195.4	8.254	8.537
sssz–9z	South Sandwich Islands Subduction Zone	-26.1799	-58.4313	195.4	51.69	37.44
sssz–10a	South Sandwich Islands Subduction Zone	-26.1563	-59.1048	212.5	32.82	15.65
sssz–10b	South Sandwich Islands Subduction Zone	-25.5335	-59.3080	212.5	10.45	6.581
sssz–10z	South Sandwich Islands Subduction Zone	-26.5817	-58.9653	212.5	54.77	42.75
sssz–11a	South Sandwich Islands Subduction Zone	-27.0794	-59.6799	224.2	33.67	15.75
sssz–11b	South Sandwich Islands Subduction Zone	-26.5460	-59.9412	224.2	11.32	5.927
sssz–11z	South Sandwich Islands Subduction Zone	-27.4245	-59.5098	224.2	57.19	43.46

C SIFT Testing

By Lindsey Wright

C.1 Purpose

Forecast models are tested with synthetic tsunami events covering a range of tsunami source locations and magnitudes. Testing is also done with selected historical tsunami events when available.

The testing of a forecast model has three objectives. The first objective is to assure that the results obtained with the NOAA's tsunami forecast system software, which has been released to the Tsunami Warning Centers for operational use, are consistent with those obtained by the researcher during the development of the forecast model. The second objective is to test the forecast model for consistency, accuracy, time efficiency, and quality of results over a range of possible tsunami locations and magnitudes. The third objective is to identify bugs and issues in need of resolution by the researcher who developed the forecast model or by the forecast system software development team before the next version release to NOAA's two Tsunami Warning Centers.

Local hardware and software applications, and tools familiar to the researcher(s), are used to run the Method of Splitting Tsunami (MOST) model during the forecast model development. The test results presented in this report lend confidence that the model performs as developed and produces the same results when initiated within the forecast system application in an operational setting as those produced by the researcher during the forecast model development. The test results assure those who rely on the Christiansted tsunami forecast model that consistent results are produced irrespective of system.

C.2 Testing Procedure

The Christiansted forecast model was tested with SIFT version 3.2. The general procedure for forecast model testing is to run a set of synthetic tsunami scenarios and a selected set of historical tsunami events through the forecast system application and compare the results with those obtained by the researcher during the forecast model development and presented in the Tsunami Forecast Model Report. Specific steps taken to test the model include:

- Identification of testing scenarios, including the standard set of synthetic events, appropriate historical events, and customized synthetic scenarios that may have been used by the researcher(s) in developing the forecast model.
- Creation of new events to represent customized synthetic scenarios used by the researcher(s) in developing the forecast model, if any.
- Submission of test model runs with the forecast system, and export of the results from A, B, and C grids, along with time series.
- Recording applicable metadata, including the specific forecast system version used for testing.

- Examination of forecast model results for instabilities in both time series and plot results.
- Comparison of forecast model results obtained through the forecast system with those obtained during the forecast model development.
- Summarization of results with specific mention of quality, consistency, and time efficiency.
- Reporting of issues identified to modeler and forecast system software development team.
- Retesting the forecast models in the forecast system when reported issues have been addressed or explained.

Synthetic model runs were tested on a DELL PowerEdge R510 computer equipped with two Xeon E5670 processors at 2.93 Ghz, each with 12 MBytes of cache and 32GB memory. The processors are hex core and support hyperthreading, resulting in the computer performing as a 24 processor core machine. Additionally, the testing computer supports 10 Gigabit Ethernet for fast network connections. This computer configuration is similar or the same as the configurations of the computers installed at the Tsunami Warning Centers so the compute times should only vary slightly.

C.3 Results

Test results from the forecast system and comparisons with the results obtained during the forecast model development are shown numerically in Table C1 and graphically in Figures C1 to C3. The results show that the minimum and maximum amplitudes and time series obtained from the forecast system agree with those obtained during the forecast model development, and that the forecast model is stable and robust, with consistent and high quality results across geographically distributed tsunami sources. The model run time (wall clock time) was 24 minutes for 10 hours of simulation time.

A suite of three synthetic events was run on the Christiansted forecast model. The modeled scenarios were stable for all cases run. The largest modeled height was 389.6 cm from the Atlantic (ATSZ 48-57) source zone. The smallest signal of 5.5 cm was recorded at the far field South Sandwich (SSSZ 1-10) source zone. The comparisons between the development cases (shown in Figures 11, 12, and 16 of the model report) and the forecast system output were consistent in shape and amplitude for all cases. The Christiansted reference point used for the forecast model development is the same as what is deployed in the forecast system, so the results can be considered valid for the three cases studied.

Table C1: Table of maximum and minimum amplitudes at Christiansted, Virgin Islands warning point for synthetic events tested using SIFT 3.2 and obtained during development.

Scenario Name	Source Zone	Tsunami Source	α (m)	SIFT Max (cm)	Development Max (cm)	SIFT Min (cm)	Development Min (cm)
ATSZ 38-47	Atlantic	A38-47, B38-47	25	201.5	203.7	-108.3	-109.3
ATSZ 48-57	Atlantic	A48-57, B48-57	25	389.6	391.7	-121.8	-123.2
SSSZ 1-10	South Sandwich	A1-10, B1-10	25	5.5	5.5	-6.5	-6.6

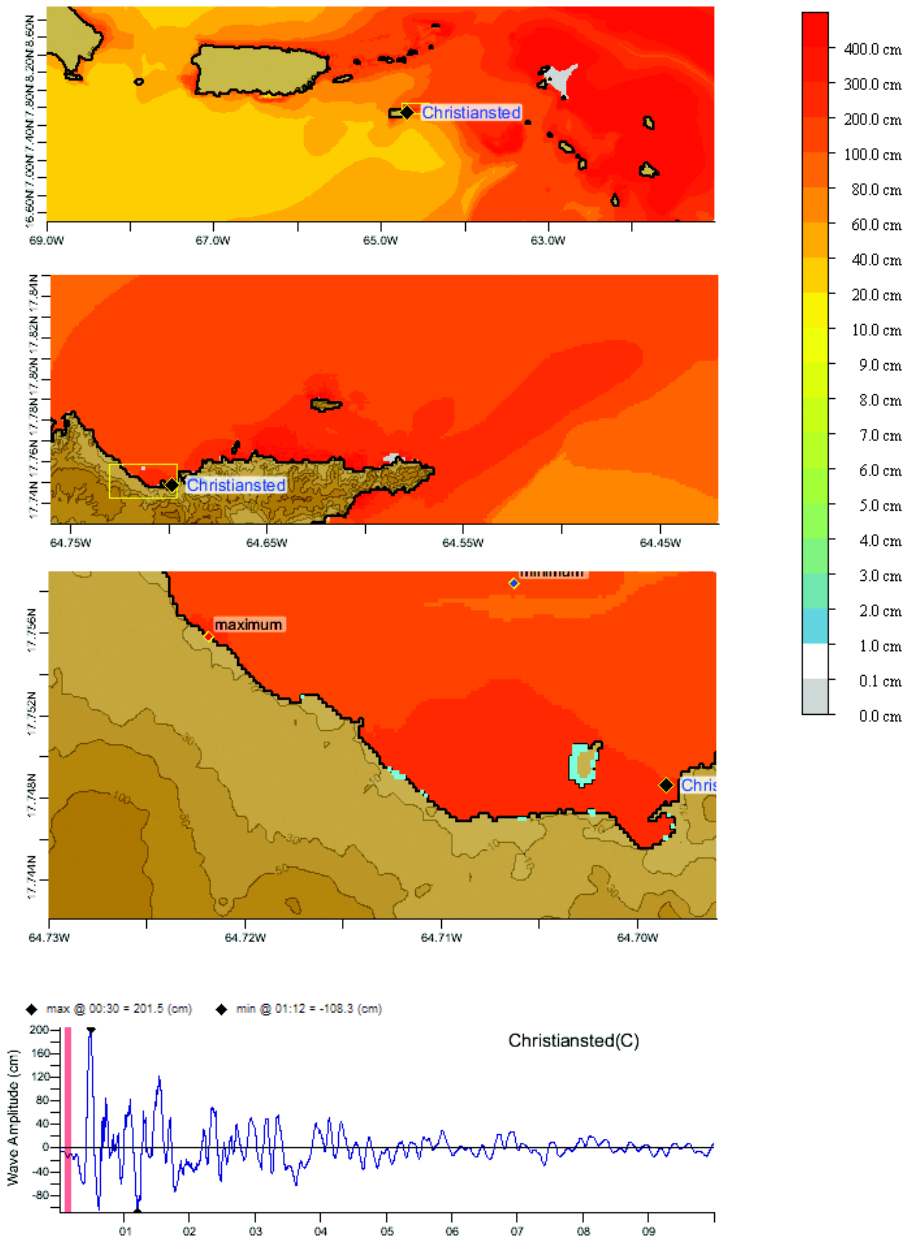

Figure C1: Response of the Christiansted forecast model to synthetic scenario ATSZ 38-47 (α=25). Plates from top to bottom are: maximum sea surface elevation for A, B, and C grids, and time series at the reference grid node.

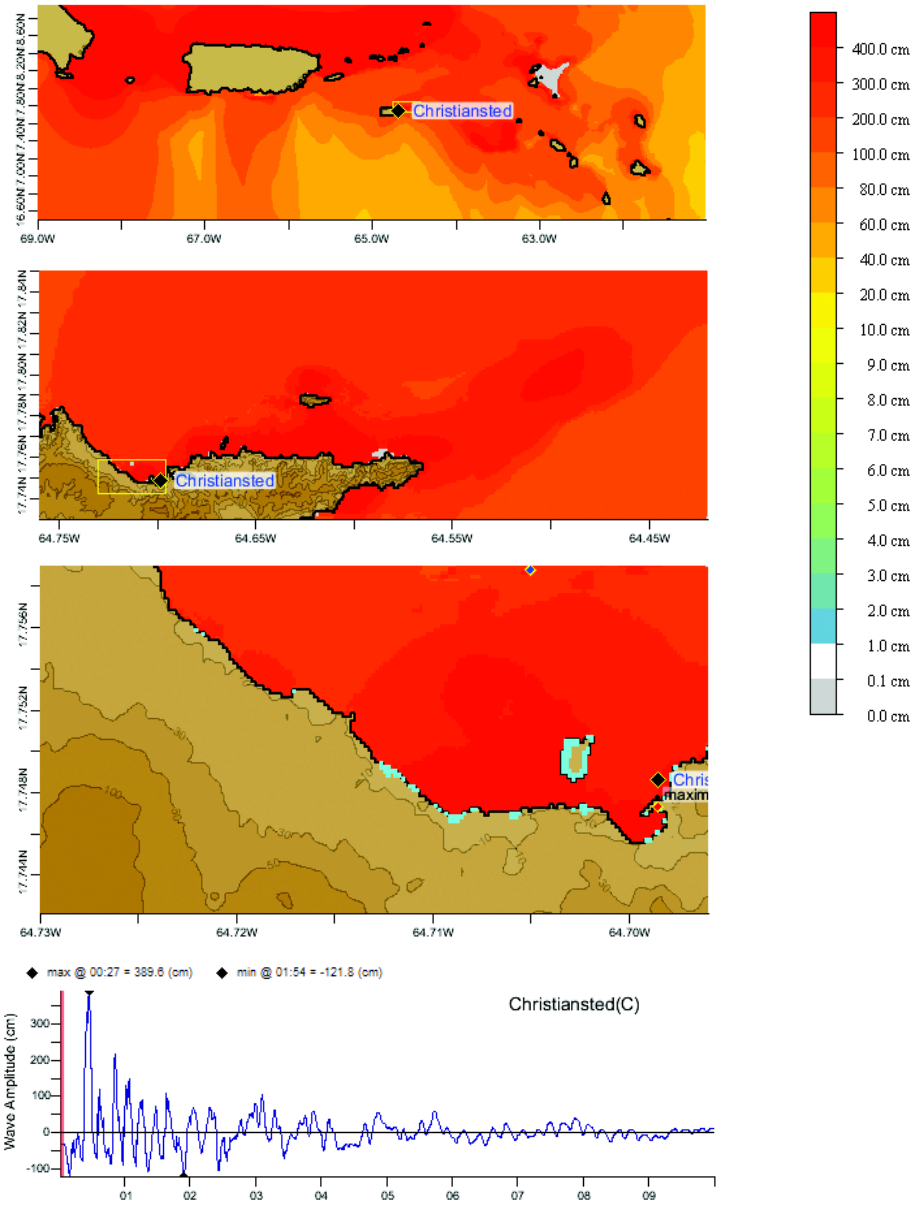

Figure C2: Response of the Christiansted forecast model to synthetic scenario ATSZ 48-57 (α=25). Plates from top to bottom are: maximum sea surface elevation for A, B, and C grids, and time series at the reference grid node.

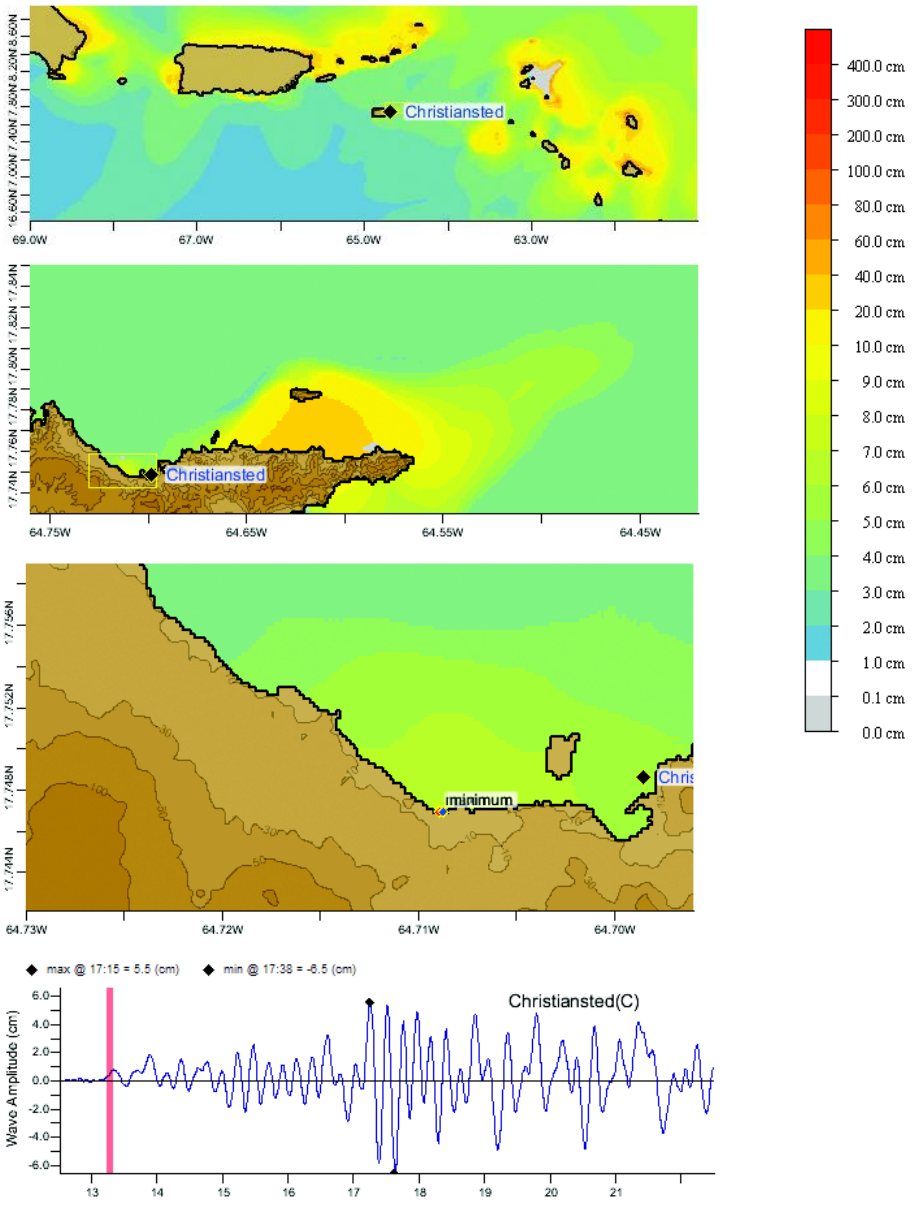

Figure C3: Response of the Christiansted forecast model to synthetic scenario SSSZ 1-10 (α=25). Plates from top to bottom are: maximum sea surface elevation for A, B, and C grids, and time series at the reference grid node.